NASA/TM—2001-210614 ARL–TR–2373

Design, Generation and Tooth Contact Analysis (TCA) of Asymmetric Face Gear Drive With Modified Geometry

Faydor L. Litvin and Alfonso Fuentes
University of Illinois at Chicago, Chicago, Illinois

J. Matthew Hawkins
Rolls-Royce, Allison Engine Company, Indianapolis, Indiana

Robert F. Handschuh
U.S. Army Research Laboratory, Glenn Research Center, Cleveland, Ohio

January 2001

The NASA STI Program Office . . . in Profile

Since its founding, NASA has been dedicated to the advancement of aeronautics and space science. The NASA Scientific and Technical Information (STI) Program Office plays a key part in helping NASA maintain this important role.

The NASA STI Program Office is operated by Langley Research Center, the Lead Center for NASA's scientific and technical information. The NASA STI Program Office provides access to the NASA STI Database, the largest collection of aeronautical and space science STI in the world. The Program Office is also NASA's institutional mechanism for disseminating the results of its research and development activities. These results are published by NASA in the NASA STI Report Series, which includes the following report types:

- TECHNICAL PUBLICATION. Reports of completed research or a major significant phase of research that present the results of NASA programs and include extensive data or theoretical analysis. Includes compilations of significant scientific and technical data and information deemed to be of continuing reference value. NASA's counterpart of peer-reviewed formal professional papers but has less stringent limitations on manuscript length and extent of graphic presentations.

- TECHNICAL MEMORANDUM. Scientific and technical findings that are preliminary or of specialized interest, e.g., quick release reports, working papers, and bibliographies that contain minimal annotation. Does not contain extensive analysis.

- CONTRACTOR REPORT. Scientific and technical findings by NASA-sponsored contractors and grantees.

- CONFERENCE PUBLICATION. Collected papers from scientific and technical conferences, symposia, seminars, or other meetings sponsored or cosponsored by NASA.

- SPECIAL PUBLICATION. Scientific, technical, or historical information from NASA programs, projects, and missions, often concerned with subjects having substantial public interest.

- TECHNICAL TRANSLATION. English-language translations of foreign scientific and technical material pertinent to NASA's mission.

Specialized services that complement the STI Program Office's diverse offerings include creating custom thesauri, building customized data bases, organizing and publishing research results . . . even providing videos.

For more information about the NASA STI Program Office, see the following:

- Access the NASA STI Program Home Page at ***http://www.sti.nasa.gov***

- E-mail your question via the Internet to help@sti.nasa.gov

- Fax your question to the NASA Access Help Desk at 301–621–0134

- Telephone the NASA Access Help Desk at 301–621–0390

- Write to:
  NASA Access Help Desk
  NASA Center for AeroSpace Information
  7121 Standard Drive
  Hanover, MD 21076

NASA/TM—2001-210614 ARL–TR–2373

Design, Generation and Tooth Contact Analysis (TCA) of Asymmetric Face Gear Drive With Modified Geometry

Faydor L. Litvin and Alfonso Fuentes
University of Illinois at Chicago, Chicago, Illinois

J. Matthew Hawkins
Rolls-Royce, Allison Engine Company, Indianapolis, Indiana

Robert F. Handschuh
U.S. Army Research Laboratory, Glenn Research Center, Cleveland, Ohio

National Aeronautics and
Space Administration

Glenn Research Center

January 2001

Acknowledgments

The authors express their deep gratitude to the Army Research Office and members of UIC–Industry Gear Research Consortium for the financial support of the performed research.

Available from

NASA Center for Aerospace Information
7121 Standard Drive
Hanover, MD 21076
Price Code: A03

National Technical Information Service
5285 Port Royal Road
Springfield, VA 22100
Price Code: A03

Available electronically at http://gltrs.grc.nasa.gov/GLTRS

DESIGN, GENERATION AND TOOTH CONTACT ANALYSIS (TCA) OF ASYMMETRIC FACE GEAR DRIVE WITH MODIFIED GEOMETRY

Faydor L. Litvin, Alfonso Fuentes
Gear Research Center
Department of Mechanical Engineering
University of Illinois at Chicago
Chicago, Illinois

J. Matthew Hawkins
Rolls-Royce, Allison Engine Co.
Indianapolis, Indiana

Robert F. Handschuh
U.S. Army Research Laboratory
National Aeronautics and Space Administration
Glenn Research Center
Cleveland, Ohio

SUMMARY

A new type of face gear drive for application in transmissions, particularly in helicopters, has been developed. The new geometry differs from the existing geometry by application of asymmetric profiles and double-crowned pinion of the face gear mesh. The paper describes the computerized design, simulation of meshing and contact, and stress analysis by finite element method. Special purpose computer codes have been developed to conduct the analysis. The analysis of this new type of face gear is illustrated with a numerical example.

NOMENCLATURE

a_i $(i = r,q)$	parabola coefficient of driving $(i = r)$ and coast $(i = q)$ sides of parabolic rack-cutter profile (fig. 13)
a_{pl}	parabola coefficient applied for tool plunging (figs. 4 and 14)
C^1	set of functions with continuous derivatives up to the first order at least
E	current value of shortest distance between the axes of the pinion and the grinding disk (fig. 4)
E_0	nominal value of E (fig. 4)
f	equation of meshing
L_i $(i = 1,2)$	inner $(i = 1)$ and outer $(i = 2)$ limiting dimensions of the face gear (fig. 12)
l_D	parameter of translation measured along axis z_k (fig. 4)
l_d, l_c	distances $\lvert Q_d O_t \rvert$ and $\lvert Q_c O_t \rvert$, respectively (figs. 5 and 7)
$\mathbf{M}_{ji}, \mathbf{L}_{ji}$	matrices 4×4 and 3×3 for transformation from S_i to S_j of point coordinates and projections of vectors

N_i ($i = s$, 1,2)	number of teeth of the shaper ($i = s$), pinion ($i = 1$), and face-gear ($i = 2$)
$\mathbf{n}_i$ ($i = t, ..., D$)	surface unit normals of the imaginary shaper rack-cutter surface ($i = t$), shaper tooth surface ($i = s$), parabolic rack-cutter surface ($i = r$), pinion tooth surface ($i = 1$), face-gear surface ($i = 2$), and grinding disk surface ($i = D$)
P	diametral pitch
$P^{(0)}$	candidate to contact point
p	circular pitch
r_a, r_p, $r_b^{(i)}$	radii of addendum, pitch, and base circles for driving ($i = d$) and coast ($i = c$) sides (figs. 3 and 8)
S	coordinate system
$s_k(k = t, b)$	width of space of the tooth ($k = t$) and the blank ($k = b$) of the generating imaginary rack-cutter (fig. 5)
T	Torque (fig. 27)
u_d, θ_d	Shaper rack-cutter surface parameters
u_r, θ_r	Pinion parabolic rack-cutter surface parameters
w_k ($k = t,b$)	Width of the space of the tooth ($k = t$) and the blank ($k = b$) of the being generated gear
x_k, y_k, z_k	Axes of coordinate system S_k
α_i ($i = d,c$)	pressure angles for asymmetric face-gear drive for driving ($i = d$) and coast ($i = c$) sides (figs. 3,5, and 7)
γ	shaft angle (fig. 16)
γ_m	complementary shaft angle (figs. 9, 10 and 12)
ΔE	change of shortest distance between the pinion and the face-gear axes (fig. 16)
Δq	axial displacement of face gear (fig. 17)
$\Delta\gamma$	change of shaft angle (fig. 17)
θ_D	surface parameter of the grinding disk
λ_t	ratio of tooth thicknesses of the imaginary asymmetric rack-cutter
ξ_r	angle applied for orientation of the pinion space in coordinate system S_1
ξ_s	angle applied for orientation of the shaper space in coordinate system S_s (fig. 8)
$\Sigma_1^{(1)}$	profile crowned pinion tooth surface
$\Sigma_1^{(2)}$	double-crowned pinion tooth surface

Σ_d	grinding disk surface
Σ_r	pinion parabolic rack-cutter surface
Σ_t	shaper rack-cutter surface
$\phi_i (i = s, 2)$	angles of rotation of the shaper ($i = s$) and the face gear ($i = 2$) performed in the process of generation of the face gear (fig. 10)
ψ_s	angle of rotation of the face-gear shaper performed in the process of generation (fig. 5)

1. INTRODUCTION

Face gear drives have found an important application in helicopter transmissions. Such gear drives, if specially designed, enable to split the torque as shown in figure 1. The technology of face gear drives, in comparison with spiral bevel gears, is more simple. However, face gear drives require hardening of gear tooth surfaces (with following grinding) to obtain tooth strength that is equivalent to the same criteria of spiral bevel gears.

The existing design of face gear drives is based on application of a conventional involute spur pinion being in contact with the conjugated face-gear (fig. 2). Errors of misalignment of such a gear drive may cause edge contact and even separation of tooth surfaces. Therefore, for the purpose of localization of bearing contact, the face gear is generated by an involute shaper with increased number N_s of teeth, where $N_s - N_1 = 1$ to 3 (N_1 is the pinion tooth number).

Investigation of face-gear drives was the subject of research accomplished by representatives of the University of Illinois at Chicago, Boeing, NASA Glenn Research Center and Lucas Western (refs. 8 to 10).

The purpose of this paper is to develop a modified geometry of face-gear drives with reduced stresses and low transmission errors. Two versions of modified geometry have been investigated and compared by analysis of stresses and simulation of meshing and contact.

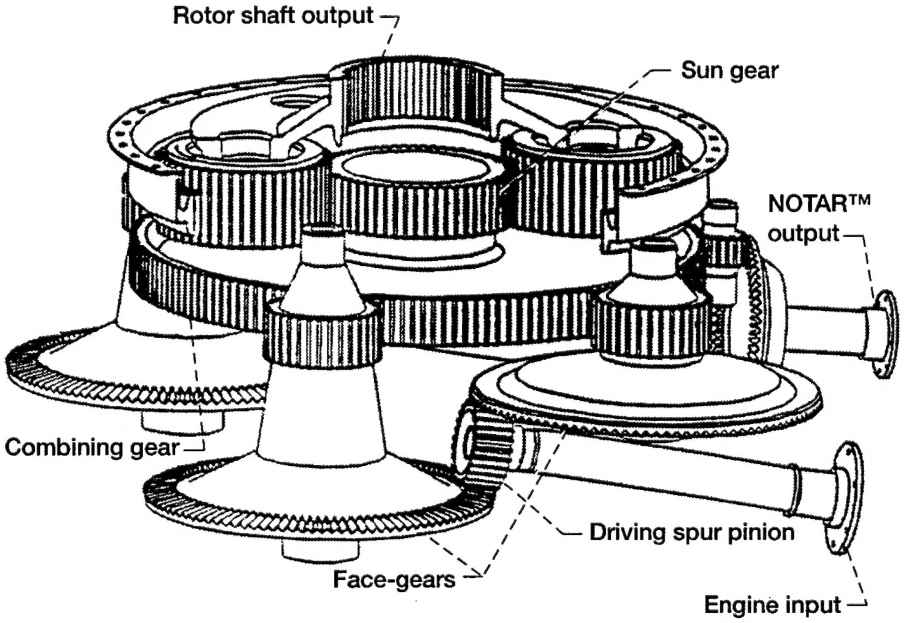

Figure 1.—Helicopter transmission with face gear drives.

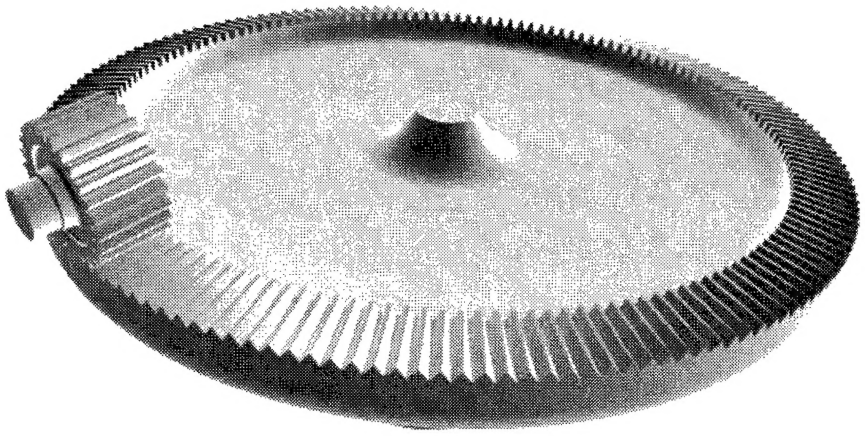

Figure 2.—Face-gear drive with spur pinion.

The modification of geometry considered in the paper is based on the following principles:

(1) The pinion is provided by tooth profiles that slightly deviate from conventional involute profiles, wherein the shaper is provided by conventional involute profiles.

(2) Profile deviation of the pinion we call profile crowning. It will be shown below (see section 5) that pinion profile crowning provides a predesigned parabolic function of transmission errors. Such a function is able to absorb almost linear discontinuous functions of transmission errors (caused by misalignment) (ref. 7) that are the source of vibration and noise.

(3) The pinion is designed with asymmetric profiles, larger pressure angle is provided for the driving side. Profiles of the shaper are asymmetric involute profiles (fig. 3).

(4) The localization of the bearing contact of face gear drive is obtained by crowning of pinion tooth surface in longitudinal direction. This can be achieved by plunging of the tool (disk or grinding worm) that generates the pinion (fig. 4).

(5) We call the pinion double crowned, if it is crowned in profile and longitudinal directions. We remind that the purpose of profile crowning is predesign of a parabolic function of transmission errors, wherein longitudinal crowning is required for localization of bearing contact.

The contents of the paper cover: (1) Development of geometry of the pinion, shaper, and face-gear; (2) Simulation of meshing and contact of the pinion and gear; (3) Stress analysis of face gear drive.

2. IMAGINARY RACK-CUTTERS

The concept of imaginary rack-cutters is applied for determination of geometry of spur pinion of the drive and the shaper that generates the face gear. We consider two approaches applied for profile crowning, described as follows.

Approach 1

A common imaginary rack-cutter is applied for generation of asymmetric profiles of the pinion and the shaper (fig. 5(a)). The asymmetry of profiles means that pressure angle α_d for the driving side is larger than the pressure angle α_c for the coast side. Parameters u_d and u_c determine the locations of current points M and N of profiles. The profiles of the rack-cutter are represented in coordinate system S_t (fig. 5(a)). During the process for generation, the rack-cutter and the pinion (shaper) perform related motions (fig. 5(b)).

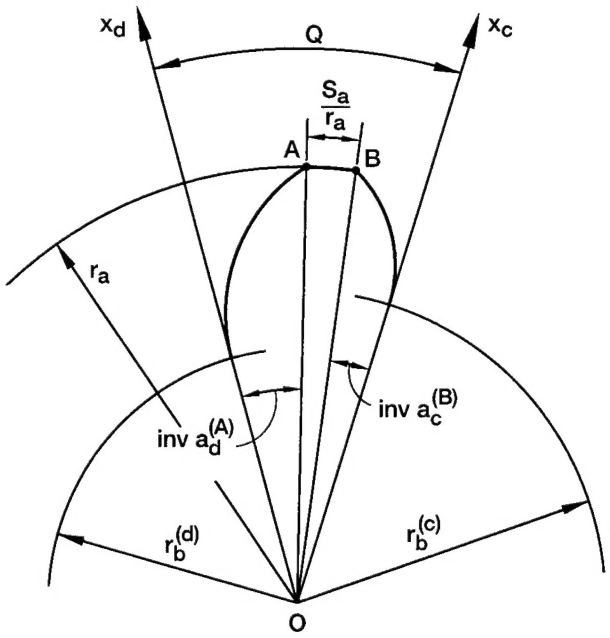

Figure 3.—Illustration of asymmetric involute profiles.

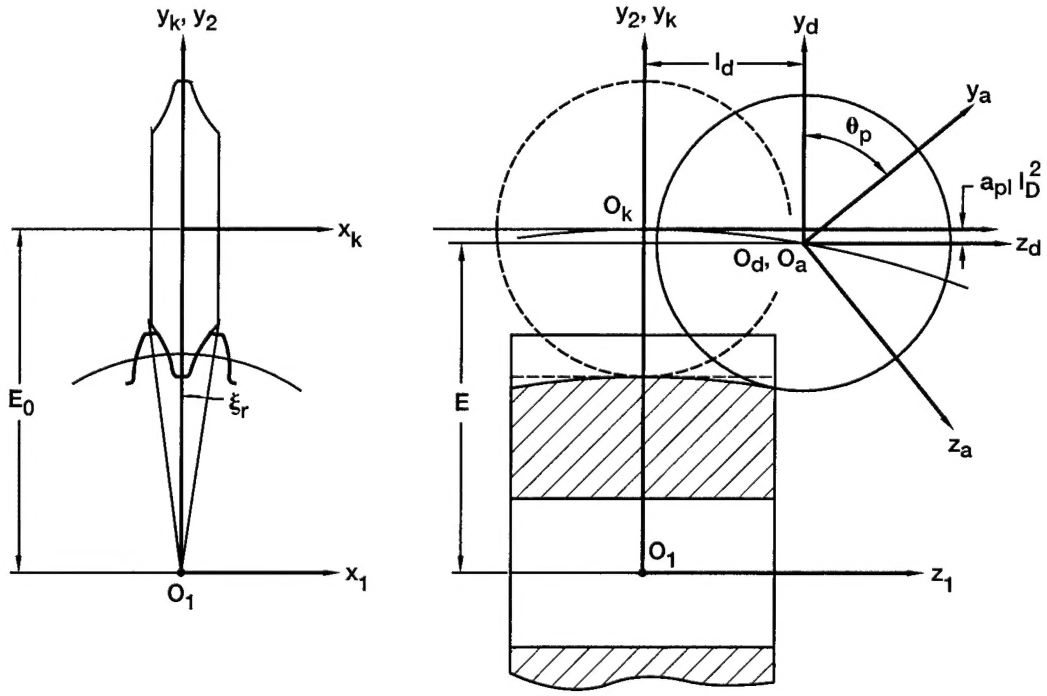

Figure 4.—Generation of pinion by plunging disk.

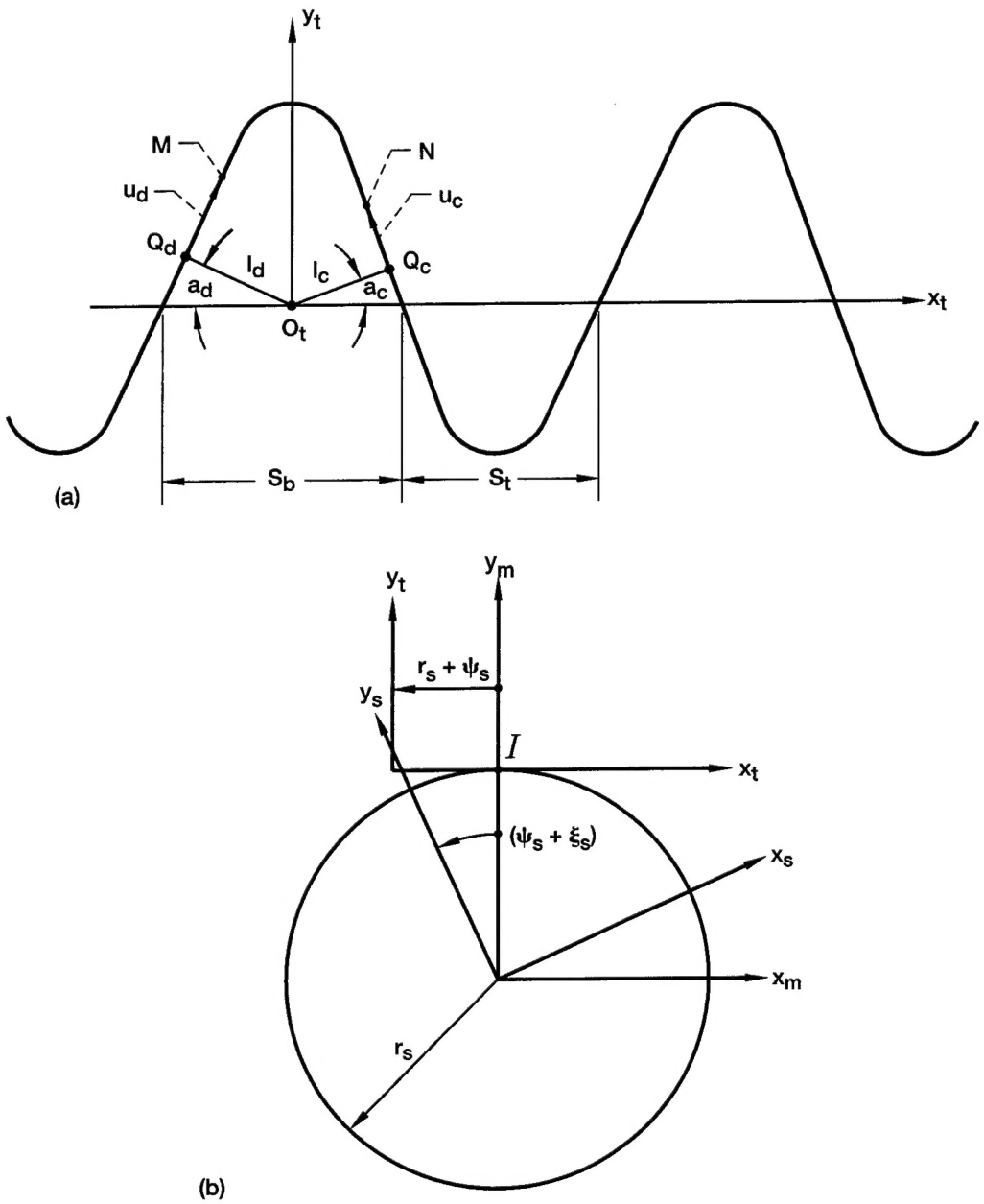

Figure 5.—For derivation of shaper and shaper rack-cutter tooth surfaces.

Profile crowning of the pinion with respect to the shaper is achieved since the number N_s of teeth of the shaper is increased with respect to the number N_1 of teeth of the pinion. The spur pinion and the face-gear generated by the shaper are in point contact and therefore the bearing contact is localized. Longitudinal crowning of the pinion, obtained as shown in figure 4, is usually not provided. The pinion and shaper generated by the common rack-cutter are in internal tangency as shown in figure 6.

There are two disadvantages of this approach:

(1) High precision of manufacturing and assembly is required to avoid separation of tooth surfaces and edge contact. The gear drive is especially sensitive to change $\Delta\gamma$ of shaft angle in the cases, wherein the axes are still intersected or become crossed.

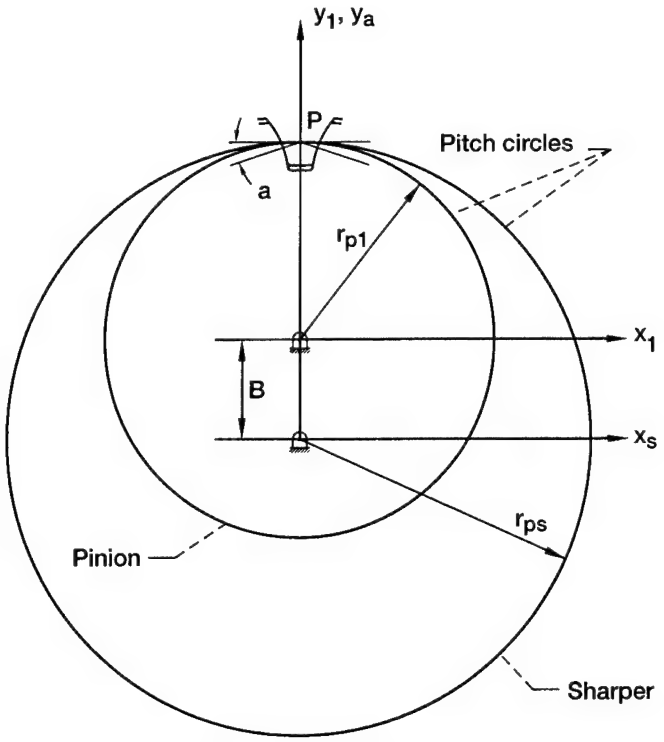

Figure 6.—Tangency of pinion and shaper tooth profiles.

(2) The dimensions of instantaneous contact ellipse are controlled by difference $(N_s - N_1)$ only. Longitudinal pinion crowning accomplished as shown in figure 4 is not applied.

The imaginary rack-cutter of asymmetric involute pinion or shaper is designed as nonstandard one (ref. 6), and its parameters s_t and s_b are related by the coefficient

$$\lambda_t = \frac{s_t}{s_b} \tag{1}$$

where λ_t is an assigned input parameter. Rolling of the pitch line with respect to the pitch circle of the being generated gear in the process of generation is provided. Therefore, we have that

$$s_t = w_b \tag{2}$$

$$s_b = w_t \tag{3}$$

where $w_k (k = t,b)$ is the width of space of the tooth and the blank of the being generated gear. It is easy to be verified that

$$s_t + w_t = s_b + w_b = p = \frac{\pi}{P} \tag{4}$$

where p and P are the circular and diametral pitches. Therefore,

$$s_t = \frac{\lambda_t p}{1+\lambda_t} = \frac{\pi\lambda_t}{(1+\lambda_t)P} \tag{5}$$

$$s_b = \frac{s_t}{\lambda} = \frac{p}{1+\lambda_t} = \frac{\pi}{(1+\lambda_t)P} \tag{6}$$

Drawnings of figure 5 yield that

$$s_b = \frac{l_d}{\cos\alpha_d} + \frac{l_c}{\cos\alpha_c} \tag{7}$$

where $l_d = |\overline{Q_d O_t}|$ and $l_c = |\overline{Q_c O_t}|$.

Radii of base circles of driving and coast side profiles are of different magnitude, since different pressure angles for both sides of profiles are assigned. Radii of base circles and operating pitch circles (centrodes) are related by the equation

$$r_b^{(i)} = r_p \cos\alpha_i = \frac{N}{2P}\cos\alpha_i \qquad (i = d, c) \tag{8}$$

where r_p is the radius of the respective centrode (of the pinion or the shaper), N is the respective number of teeth (of the pinion or the shaper), P is the diametral pitch, and α_i is the pressure angle of the side considered.

Henceforth we shall consider four base circles: two for the driving and coast sides of the pinion and two for the respective sides of the shaper. There are two values α_d and α_c of the pressure angles, for the driving side and coast sides, and α_d (respectively, α_c) is the same for the pinion and the shaper. The pair of base circles of the pinion (respectively, of the shaper) have a common center.

Approach 2

This approach is based on following considerations:

(1) Two different imaginary rack-cutter are applied for generation of the shaper and the spur pinion (fig. 7).

(2) The shaper rack-cutter is provided with asymmetric straight-line profiles and therefore it will generate asymmetric involute shaper profiles. The geometry of the straight-line profile rack-cutter has been discussed above.

(3) The pinion rack-cutter is provided with parabolic profiles, asymmetric as well, that slightly deviate from straight-line profiles of the shaper (see section 5). This enables, as shown below, to obtain a predesigned parabolic function of transmission errors that can absorb linear functions of transmission errors caused by misalignment (ref. 7).

(4) In addition to profile crowning, longitudinal crowning is provided by tool plunging in the process of generation of the pinion (fig. 4).

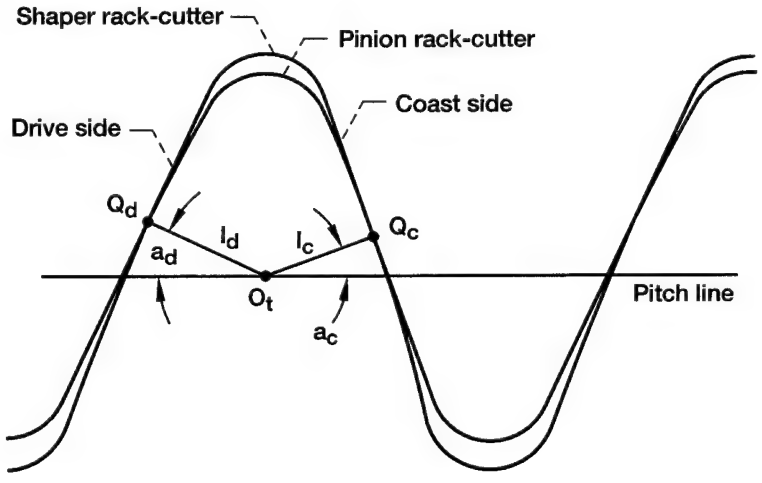

Figure 7.—Shaper and pinion rack-cutters.

3. GEOMETRY OF FACE-GEAR TOOTH SURFACES

The face-gear tooth surfaces Σ_2 are generated by asymmetric involute shaper. The shaper is generated by an asymmetric rack-cutter shown in figure 5. The derivation of face-gear tooth surfaces is based on consideration of two following enveloping processes applied in following sequence:

(1) The shaper tooth surfaces Σ_s are determined as envelopes to rack cutter surfaces shown in figure 5.
(2) Then, the sought-for tooth surfaces of the face-gear are determined as envelopes to shaper tooth surfaces.

Derivation of Shaper Tooth Surface

Figure 5(a) shows the shaper rack-cutter profiles. Figure 5(b) is the schematic of generation of shaper tooth surface by the rack cutter.

The derivations below correspond to generation of driving tooth surface. Plane $y_t = 0$ and cylinder of radius r_s are the axodes in the process for generation (fig. 5(b)). Parameters u_d and θ_d are the rack-cutter surface parameters wherein u_d is measured from point Q_d, and θ_d (not shown in fig. 5(a)) is measured from Q_d in the direction that is parallel to axis z_t.

Rack-cutter surface Σ_t is represented in coordinate system S_t by the following vector function $\mathbf{r}_t(u_d,\theta_d)$

$$\mathbf{r}_t = \begin{bmatrix} u_d \sin\alpha_d - l_d \cos\alpha_d \\ u_d \cos\alpha_d + l_d \sin\alpha_d \\ \theta_d \\ 1 \end{bmatrix} \tag{9}$$

Here: α_d is the pressure angle of driving profile; $l_d = |\overline{Q_d O_t}|$.

The rack-cutter surface unit normal is represented in as

$$\mathbf{n}_t = \begin{bmatrix} \cos\alpha_d & -\sin\alpha_d & 0 \end{bmatrix}^T \tag{10}$$

During the process of shaper generation, the rack-cutter and the shaper perform related translational and rotational motions as shown in figure 5(b). Axis I-I is the instantaneous axis of rotation.

The shaper tooth surface Σ_s is represented as follows

$$\mathbf{r}_s = (u_d, \theta_d, \psi_s) = \mathbf{M}_{st}(\psi_s)\mathbf{r}_t(u_d, \theta_d) \tag{11}$$

$$f_{st}(u_d, \psi_s) = u_d - \psi_s r_s \sin\alpha_d = 0 \tag{12}$$

where

$$\mathbf{M}_{st} = \begin{bmatrix} \cos(\psi_s + \xi_s) & \sin(\psi_s + \xi_s) & 0 & r_s(\sin(\psi_s + \xi_s) - \psi_s \cos(\psi_s + \xi_s)) \\ -\sin(\psi_s + \xi_s) & \cos(\psi_s + \xi_s) & 0 & r_s(\cos(\psi_s + \xi_s) + \psi_s \sin(\psi_s + \xi_s)) \\ 0 & 0 & 1 & 0 \\ 0 & 0 & 0 & 1 \end{bmatrix} \tag{13}$$

Angle ξ_s is a fixed angle introduced to relate orientation of coordinate system S_s with the shaper space as shown in figure 8.

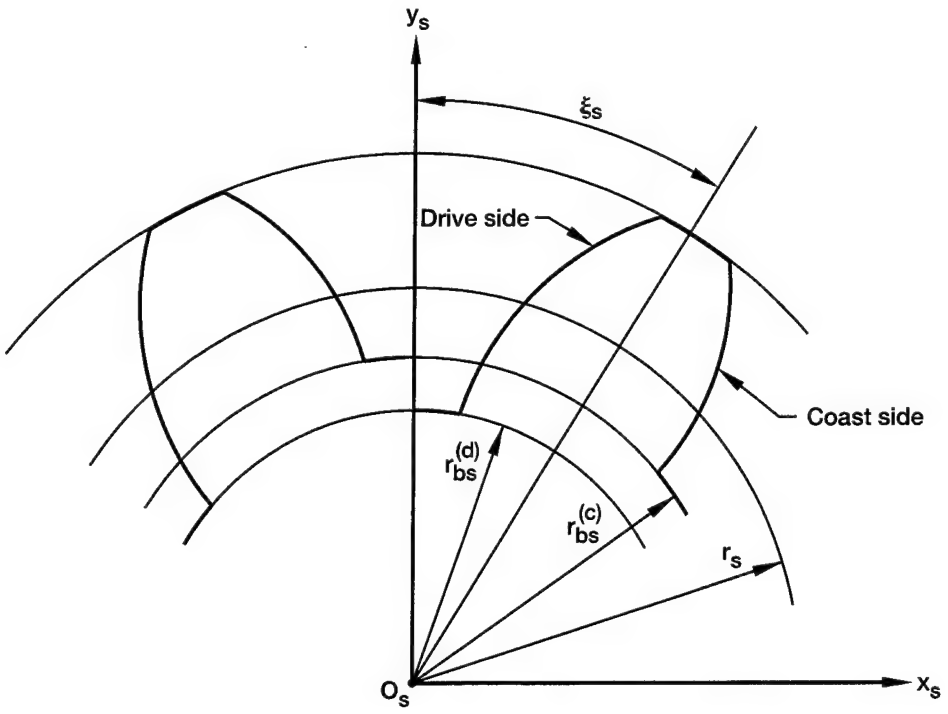

Figure 8.—Orientation of coordinate system S_s with respect to shaper space.

Equation (11) represents in S_s the family of rack-cutter surfaces. Equation (12) is the equation of meshing of shaper rack-cutter and shaper, that may be derived as represented in reference 7.

Equations (11) and (12), considered simultaneously, represent shaper surface Σ_s by three related parameters. Taking into account that equations (11) and (12) are linear with respect to parameters u_d and θ_d, it is easy eliminate one of them and represent surface Σ_s in terms of two parameters.

Derivations similar to discussed above enable to derive the coast side surface of shaper.

Derivation of Face-Gear Tooth Surface Σ_2: Surface Σ_2 is the envelope to the family of shaper tooth surfaces represented in coordinate system S_2. Generation of Σ_2 by the shaper is represented schematically in figure 9. The shaper and the face-gear perform rotations about axes z_s and z_2 related as $\phi_2/\phi_s = N_s/N_2$.

We apply for derivation of Σ_2 coordinate systems shown in figure 10. Here: (1) movable coordinate systems S_s and S_2 are rigidly connected to the shaper and face-gear, respectively; (2) fixed coordinate system S_m is rigidly connected to the housing of the generating equipment, and S_p is an auxiliary fixed coordinate system.

The shaper tooth surface Σ_s, after transformations of equations (11) and (12), is represented in coordinate system S_s by the following vector equation

$$\mathbf{r}_s(u_d,\theta_d,\psi_s(u_d)) = \mathbf{r}_s(u_d,\theta_d) = \begin{bmatrix} x_s(u_d,\psi_s(u_d)) \\ y_s(u_d,\psi_s(u_d)) \\ \theta_d \\ 1 \end{bmatrix} \tag{14}$$

Here:

$$\begin{aligned} x_s(u_d,\psi_s(u_d)) = {} & (u_d \sin\alpha_d - l_d \cos\alpha_d)\cos(\psi_s + \xi_s) + \\ & (u_d \cos\alpha_d + l_d \sin\alpha_d)\sin(\psi_s + \xi_s) + \\ & r_s(\sin(\psi_s + \xi_s) - \psi_s \cos(\psi_s + \xi_s) \end{aligned} \tag{15}$$

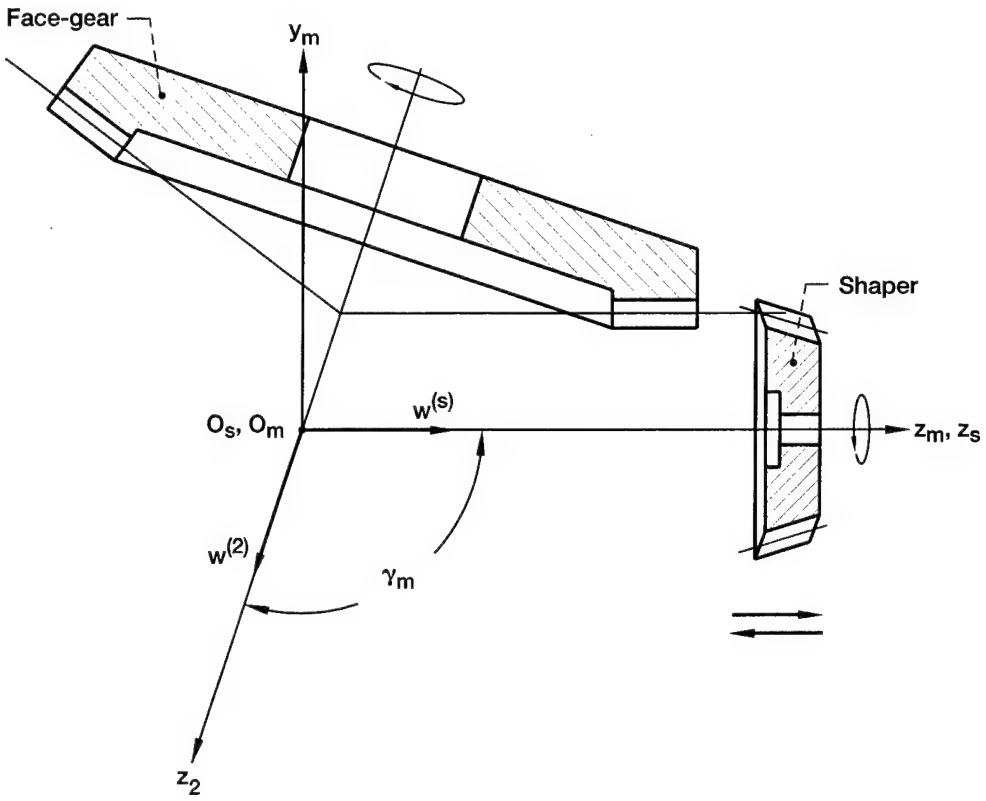

Figure 9.—Schematic of generation of face-gear.

$$\begin{aligned} y_s(u_d,\psi_s(u_d)) = {} & (u_d\cos\alpha_d + l_d\sin\alpha_d)\cos(\psi_s+\xi_s) - \\ & (u_d\sin\alpha_d - l_d\cos\alpha_d)\sin(\psi_s+\xi_s) + \\ & r_s(\cos(\psi_s+\xi_s)+\psi_s\sin(\psi_s+\xi_s)) \end{aligned} \tag{16}$$

Parameter ψ_s can be replaced by $u_d/(r_s \sin \alpha_d)$.
The unit normal to shaper tooth surface $\mathbf{n}_s(\psi_s(u_d))$ is represented as

$$\mathbf{n}_s(\psi_s(u_d)) = \frac{\dfrac{\partial \mathbf{r}_s}{\partial u_d}\times\dfrac{\partial \mathbf{r}_s}{\partial \theta_d}}{\left|\dfrac{\partial \mathbf{r}_s}{\partial u_d}\times\dfrac{\partial \mathbf{r}_s}{\partial \theta_d}\right|} = \begin{bmatrix} \cos(\alpha_d+\psi_s+\xi_s) \\ -\sin(\alpha_d+\psi_s+\xi_s) \\ 0 \end{bmatrix} \tag{17}$$

Surface Σ_2 of the face-gear is determined as the envelope to family of shaper surfaces Σ_s by the following equations

$$\mathbf{r}_2(u_d,\theta_d,\phi_s) = \mathbf{M}_{2s}(\phi_s)\mathbf{r}_s(u_d,\theta_d) \tag{18}$$

$$f_{2s}(u_d,\theta_d,\phi_s) = r_s\cos\alpha_d(1-m_{2s}\cos\gamma_m) - m_{2s}\theta_d\sin\gamma_m\cos(\alpha_d+\psi_s+\xi_s-\phi_s) = 0 \tag{19}$$

Equation (18) represents in S_2 the family of surfaces Σ_s. Equation (19) is the equation of meshing. Matrix $\mathbf{M}_{2s}$ describes the coordinate transformation from S_s to S_2 and is represented as

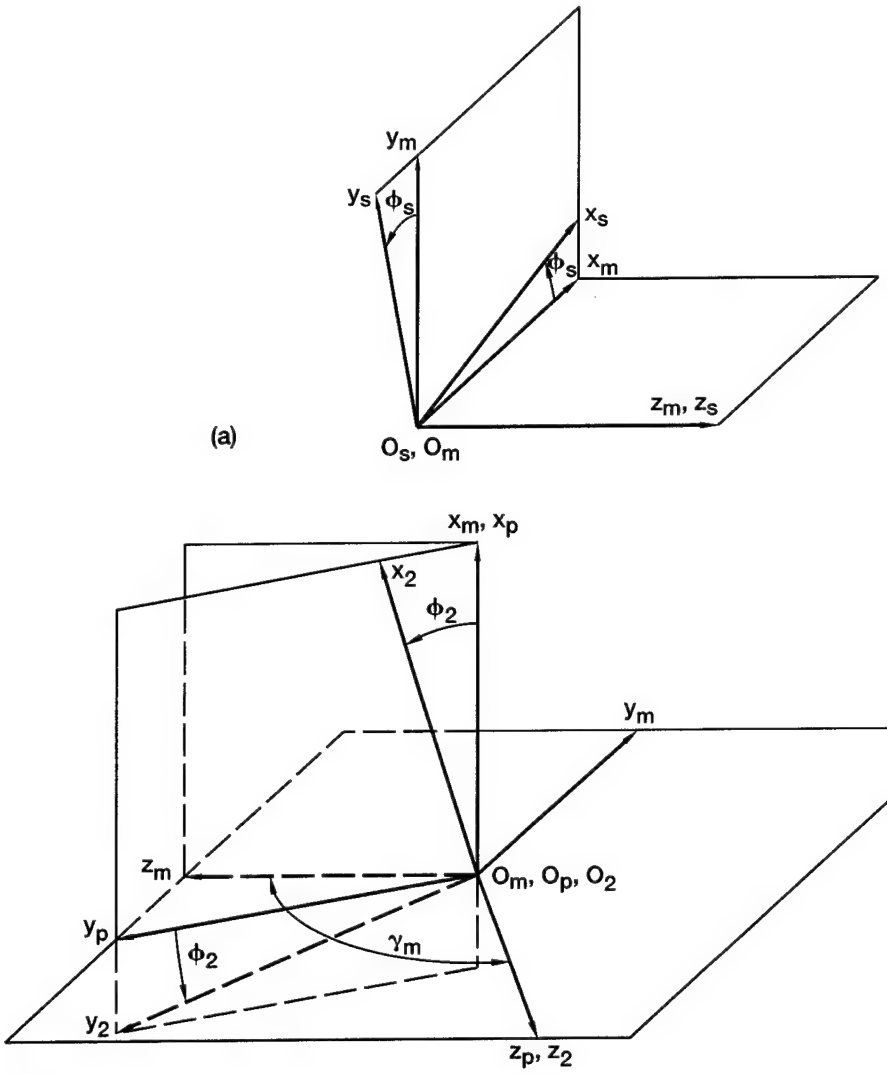

Figure 10.—Coordinate systems applied for generation of face-gear tooth surface Σ_2. (a) Illustration of rotation of shaper. (b) Illustration of rotation of face-gear.

$$\mathbf{M}_{2s} = \begin{bmatrix} \cos\phi_s \cos\phi_2 & -\sin\phi_s \cos\phi_2 & \sin\gamma_m \sin\phi_2 & 0 \\ +\cos\gamma_m \sin\phi_s \sin\phi_2 & +\cos\gamma_m \cos\phi_s \sin\phi_2 & & \\ -\cos\phi_s \sin\phi_2 & \sin\phi_s \sin\phi_2 & \sin\gamma_m \cos\phi_2 & 0 \\ +\cos\gamma_m \sin\phi_s \cos\phi_2 & +\cos\gamma_m \cos\phi_s \cos\phi_2 & & \\ -\sin\gamma_m \sin\phi_s & -\sin\gamma_m \cos\phi_s & \cos\gamma_m & 0 \\ 0 & 0 & 0 & 1 \end{bmatrix} \tag{20}$$

The unit normal to the face-gear surface Σ_2 is represented in S_2 as

$$\mathbf{n}_2(u_d, \theta_d, \phi_s) = \mathbf{L}_{2s}(\phi_s, \theta_d)\mathbf{n}_s(u_d) \tag{21}$$

The 3×3 matrix $\mathbf{L}_{2s}$ in equation (21) and in similar derivations is a submatrix of the 4×4 matrix $\mathbf{M}_{2s}$. It is obtained by elimination of the last row and column of $\mathbf{M}_{2s}$. Elements of matrix $\mathbf{L}_{2s}$ represent the direction cosines formed by respective axes of coordinate systems S_2 and S_s (ref. 7).

4. AVOIDANCE OF UNDERCUTTING AND POINTING

The structure of the tooth of symmetric face-gear is shown in figure 11. The tooth surface is covered with contact lines L_{2s} between the face-gear and shaper surfaces. The fillet surface is generated by the edge of the addendum of the shaper. Line L^* is the line of tangency of the contact lines L_{2s} with the fillet surface.

Dimension of L_1 and L_2 (fig. 12) determine the zones free of undercutting and pointing, respectively. Determination of L_1 and L_2 is represented in reference 7.

For the case of an asymmetric face-gear, undercutting conditions have to be determined for both tooth sides, the driving one and the coast side of the tooth. Undercutting will ocurr at the side with lower pressure angle. Therefore, undercutting conditions for the coast side of the tooth surface will limit the inner limiting parameter L_1 (fig. 12).

Determination of pointing conditions of symmetric face-gear drive, as discussed in reference 7, can be used to determine limiting outer dimension L_2 of the face-gear (fig. 12). For asymmetric face-gear teeth, the location of tooth pointing area may be determined considering the intersection of the driving side and the coast side tooth surfaces at the top land of the tooth. A computer program to the solution of this problem has been developed. Increase of the pressure angle of the driving side decreases the limiting outer dimension L_2 of the face-gear.

5. GEOMETRY OF DOUBLE-CROWNED PINION TOOTH SURFACES

Formation of double-crowned pinion tooth surface is accomplished as follows:

Step 1.—We consider as given surface Σ_r of a parabolic rack-cutter. Surface Σ_r generates pinion tooth surface $\Sigma_1^{(1)}$ that is deviated in profile direction from a conventional involute tooth surface. This is achieved since pinion rack-cutter profile is a parabola but not a straight line (fig. 13(a)).

Step 2.—Considering as known profile crowned pinion tooth surface $\Sigma_1^{(1)}$, we may determine the cross-section profile of $\Sigma_1^{(1)}$ that coincides with the axial profile of disk surface Σ_D. Surface Σ_D is a surface of revolution formed by rotation of disk axial profile about the disk axis.

Step 3.—We consider as known surface Σ_D of the grinding disk determined in Step 2. The double-crowned pinion tooth surface is generated as the envelope to family of disk surface Σ_D as follows:

The motion of disk with respect to the pinion is performed as combination of: (1) translational motion along the axis z_k, rigidly connected to the pinion, and is parallel to axis z_1 of the pinion coordinate system (fig. 14); (2) plunging translational motion accomplished in the direction of y_k axis, along the shortest distance E_0 between the axes of the pinion and the disk (fig. 4). The plunging motion is executed in accordance to the equation

$$E = E_0 - a_{pl} l_D^2 \tag{22}$$

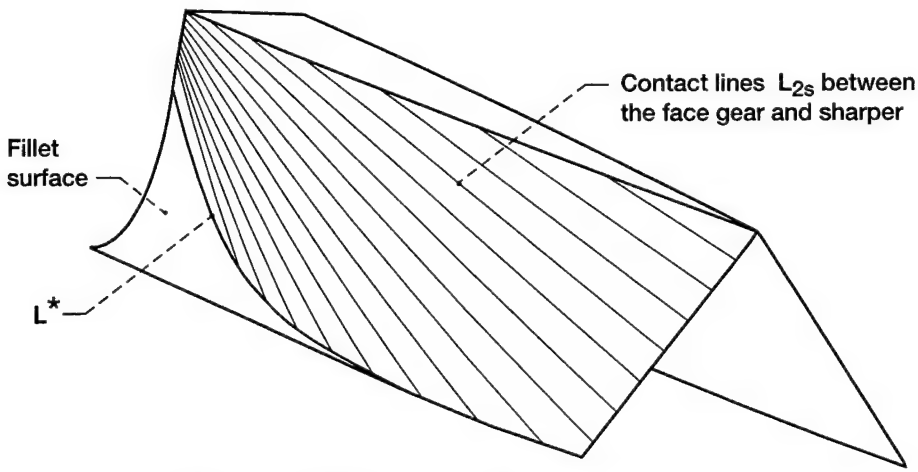

Figure 11.—Structure of the tooth of symmetric face-gear.

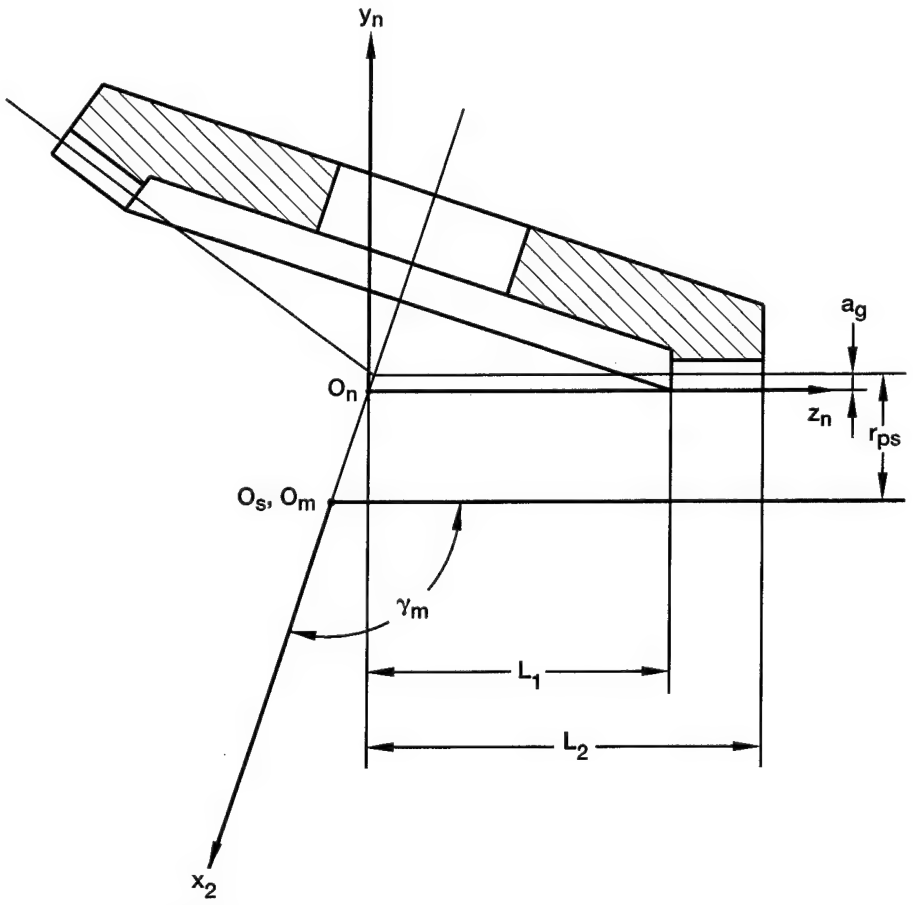

Figure 12.—Limiting dimensions L_1 and L_2 of face-gear.

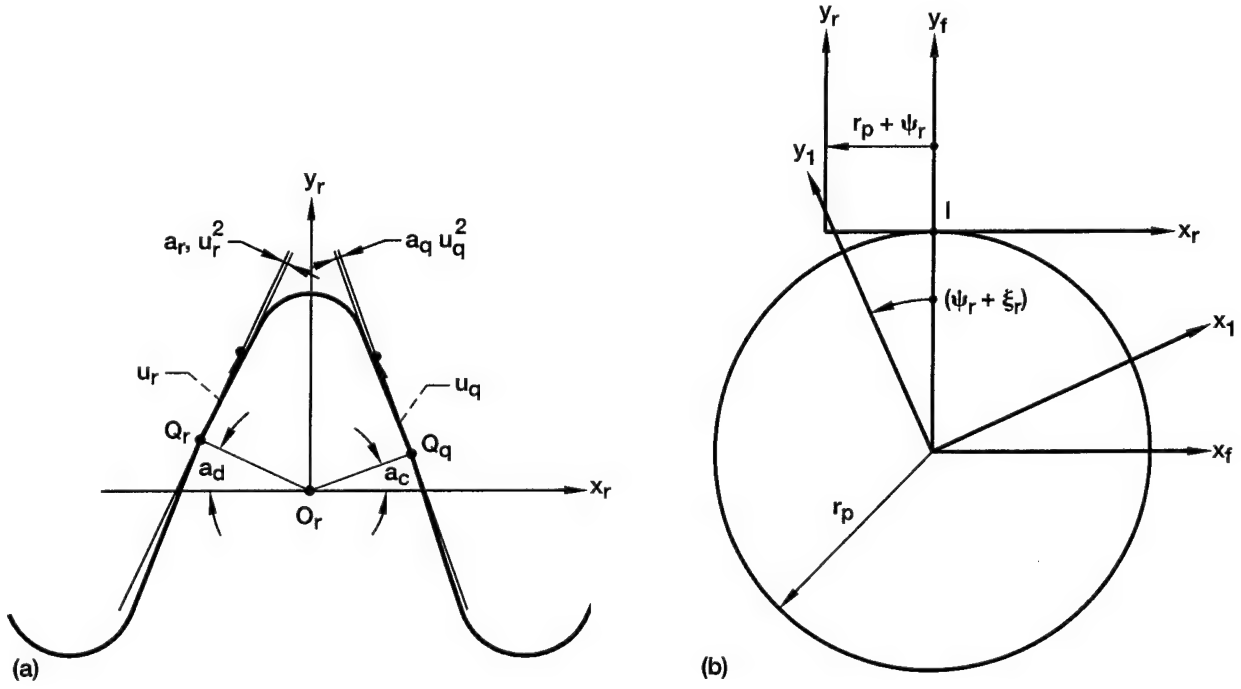

Figure 13.—Applied coordinate systems for generation of the profile of the grinding disk.

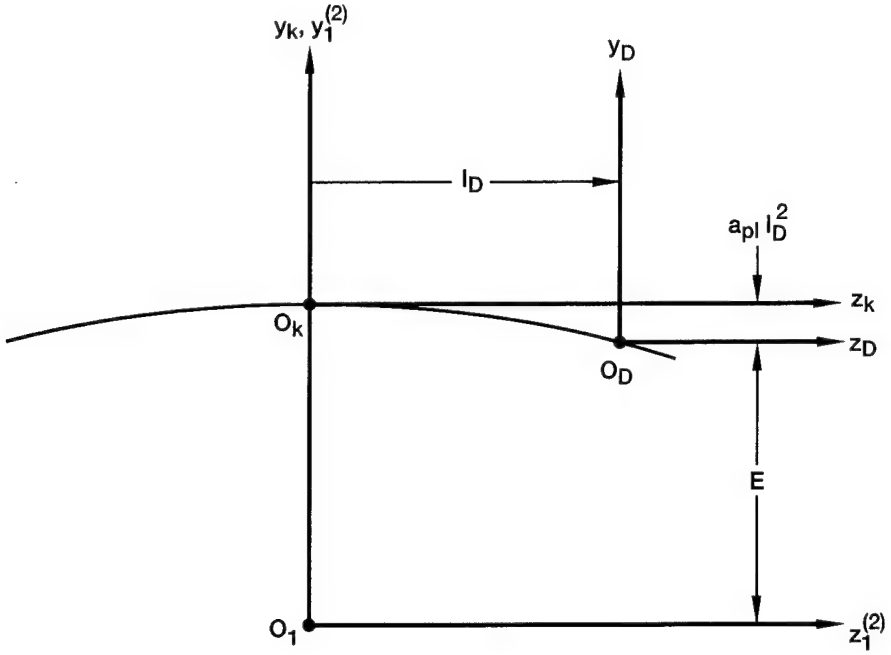

Figure 14.—For generation of pinion double-crowned surface $\Sigma_1^{(2)}$.

Here, l_D determines the translation along the pinion axis; a_{pl} is the parabola coefficient of the longitudinal plunging trajectory; E_0 and E are the initial and current magnitudes of shortest distance between the axes of rotation of the pinion and grinding disk.

The derivation below corresponds to the driving side of the pinion tooth surface. Similar derivations may be accomplished for determination the coast side of the pinion tooth surface.

Pinion Parabolic Rack-Cutter Surface

Figure 13(a) shows the pinion parabolic rack-cutter profile. Figure 13(b) is the schematic generation of the pinion tooth surface $\Sigma_1^{(1)}$.

Plane $y_r = 0$ and cylinder of radius r_p are the axodes in the process of generation as shown in figure 13. Parameter u_r and θ_r are the parabolic rack-cutter surface parameters, wherein u_r is measured from point Q_r along the tangent to the parabola at Q_r, and θ_r (not shown in fig. 13(a)) is measured from Q_r in the direction that is parallel to axis z_r.

Parabolic rack-cutter surface Σ_r is represented in coordinate system S_r by the following vector function $\mathbf{r}_r(u_r,\theta_r)$

$$\mathbf{r}_r(u_r,\theta_r) = \begin{bmatrix} u_r \sin\alpha_d - l_d \cos\alpha_d + a_r u_r^2 \cos\alpha_d \\ u_r \cos\alpha_d + l_d \sin\alpha_d - a_r u_r^2 \sin\alpha_d \\ \theta_r \\ 1 \end{bmatrix} \tag{23}$$

where a_r is the parabola coefficient of the parabolic rack-cutter profile.

The parabolic rack-cutter unit normal $\mathbf{n}_r(u_r)$ is represented in S_r as

$$\mathbf{n}_r(u_r) = \begin{bmatrix} \cos\alpha_d - 2a_r u_r \sin\alpha_d \\ -\sin\alpha_d - 2a_r u_r \cos\alpha_d \\ 0 \end{bmatrix} \frac{1}{\sqrt{1+4a_r^2 u_r^2}} \tag{24}$$

Pinion Profile Crowned Tooth Surface

During the process of pinion generation, the parabolic rack-cutter and the being-generated pinion perform related translational and rotational motions as shown in figure 13(b).

The profile crowned pinion tooth surface $\Sigma_1^{(1)}$ is represented as follows

$$\mathbf{r}_1^{(1)}(u_r, \theta_r, \psi_r) = \mathbf{M}_{1r}(\psi_r)\mathbf{r}_r(u_r, \theta_r) \tag{25}$$

$$f_{1r}(u_r, \psi_r) = u_r - 2a_r u_r l_d + 2a_r^2 u_r^3 - r_p \psi_r (2a_r u_r \cos\alpha_d + \sin\alpha_d) = 0 \tag{26}$$

where

$$\mathbf{M}_{1r} = \begin{bmatrix} \cos(\psi_r + \xi_r) & \sin(\psi_r + \xi_r) & 0 & r_p(\sin(\psi_r + \xi_r) - \psi_r \cos(\psi_r + \xi_r)) \\ -\sin(\psi_r + \xi_r) & \cos(\psi_r + \xi_r) & 0 & r_p(\cos(\psi_r + \xi_r) + \psi_r \sin(\psi_r + \xi_r)) \\ 0 & 0 & 1 & 0 \\ 0 & 0 & 0 & 1 \end{bmatrix} \tag{27}$$

Matrix $\mathbf{M}_{1r}$ describes the coordinate transformation from S_r to S_1. Application of angle ξ_r enables the orientation of axis y_1 (fig. 4) with the pinion space, as it was done for the shaper (fig. 8).

Equation (25) represents in S_1 the family of rack-cutter surfaces Σ_r. Equation (26) is the equation of meshing of Σ_r and $\Sigma_1^{(1)}$. Equations (25) and (26), considered simultaneously, determine the profile crowned pinion tooth surface $\Sigma_1^{(1)}$.

The unit normal to the profile crowned pinion tooth surface $\mathbf{n}_1(u_r, \psi_r)$ is determined as

$$\mathbf{n}_1(u_r, \psi_r) = \mathbf{L}_{1r}(\psi_r)\mathbf{n}_r(u_r) \tag{28}$$

Disk Surface

The procedure of derivation of grinding disk surface Σ_D is as follows:

(1) Taking in equation (25) $\theta_r = 0$, we obtain the pinion tooth profile as the cross-section of $\Sigma_1^{(1)}$ by plane $z_1 = 0$. Equation (26) is linear with respect to ψ_r and the cross-section profile may be determined by vector function $\mathbf{r}_1(u_r)$.

(2) We apply for derivation of Σ_D the following coordinate systems: (a) S_1 that is rigidly connected to pinion (fig. 15(a)), and (b) S_a that is a coordinate system related to the grinding disk, where we represent the disk axial profile located in plane (y_a, z_a). The disk axial profile coincides with pinion cross-section profile and is determined in S_a by vector function

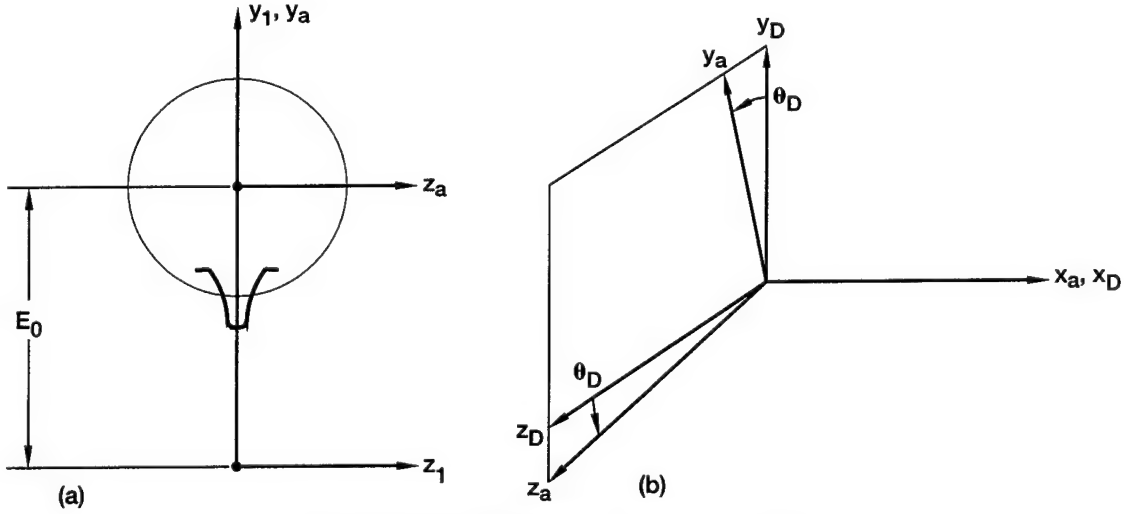

Figure 15.—For generation of disk surface Σ_D.

$$\mathbf{r}_a(u_r) = \mathbf{M}_{a1}\mathbf{r}_1(u_r) \tag{29}$$

where

$$\mathbf{M}_{a1} = \begin{bmatrix} 1 & 0 & 0 & 0 \\ 0 & 1 & 0 & -E_0 \\ 0 & 0 & 1 & 0 \\ 0 & 0 & 0 & 1 \end{bmatrix} \tag{30}$$

(3) The disk surface Σ_D is generated by its axial profile wherein coordinate system S_a is rotated about axis x_D (fig. 15(b)). Disk surface Σ_D is represented in S_D as follows

$$\mathbf{r}_D(u_r, \theta_D) = \mathbf{M}_{Da}(\theta_D)\mathbf{M}_{a1}\mathbf{r}_1(u_r) \tag{31}$$

where

$$\mathbf{M}_{Da}(\theta_D) = \begin{bmatrix} 1 & 0 & 0 & 0 \\ 0 & \cos\theta_D & -\sin\theta_D & 0 \\ 0 & \sin\theta_D & \cos\theta_D & 0 \\ 0 & 0 & 0 & 1 \end{bmatrix} \tag{32}$$

Then, we obtain

$$\mathbf{r}_D(u_r, \theta_D) = \begin{bmatrix} x_D(u_r, \theta_D) \\ y_D(u_r, \theta_D) \\ z_D(u_r, \theta_D) \end{bmatrix} \tag{33}$$

where

$$\begin{aligned} x_D(u_r, \theta_D) = {} & r_p \sin(\psi_r + \xi_r) - r_p\psi_r \cos(\psi_r + \xi_r) + \\ & l_D \cos(\alpha_d + \psi_r + \xi_r) + u_r \sin(\alpha_d + \psi_r + \xi_r) + \\ & a_r u_r^2 \cos(\alpha_d + \psi_r + \xi_r) \end{aligned} \tag{34}$$

$$\begin{aligned} y_D(u_r, \theta_D) = {} & \cos\theta_D(-E_0 + r_p \cos(\psi_r + \xi_r) + r_p\psi_r \sin(\psi_r + \xi_r) + \\ & l_D \sin(\alpha_d + \psi_r + \xi_r) + u_r \cos(\alpha_d + \psi_r + \xi_r) - \\ & a_r u_r^2 \sin(\alpha_d + \psi_r + \xi_r)) \end{aligned} \tag{35}$$

$$\begin{aligned} z_D(u_r, \theta_D) = {} & \sin\theta_D(-E_0 + r_p \cos(\psi_r + \xi_r) + r_p\psi_r \sin(\psi_r + \xi_r) + \\ & l_D \sin(\alpha_d + \psi_r + \xi_r) + u_r \cos(\alpha_d + \psi_r + \xi_r) - \\ & a_r u_r^2 \sin(\alpha_d + \psi_r + \xi_r)) \end{aligned} \tag{36}$$

The unit normal to the disk surface $\mathbf{n}_D(u_r, \theta_D)$ is obtained as

$$\mathbf{n}_D(u_r, \theta_D) = \mathbf{L}_{Da}(\theta_D)\mathbf{L}_{a1}\mathbf{n}_1(u_r) \tag{37}$$

where $\mathbf{n}_1(u_r)$ is the unit normal to the disk axial profile given by

$$\mathbf{n}_1(u_r) = \frac{\frac{\partial \mathbf{r}_1}{\partial u_r} \times \mathbf{k}_1}{\left| \frac{\partial \mathbf{r}_1}{\partial u_r} \times \mathbf{k}_1 \right|} \tag{38}$$

and $\mathbf{k}_1$ is the unit vector of the coordinate system S_1 in the direction of axis z_1 given by

$$\mathbf{k}_1 = [0 \quad 0 \quad 1]^T \tag{39}$$

Double-Crowned Pinion Surface

We remind that $\Sigma_1^{(2)}$ is generated as the envelope to family of disk surfaces Σ_D wherein the disk performs translational and plunging motions as shown in figure 4. We apply for derivation of $\Sigma_1^{(2)}$ the following coordinate systems (fig. 14): (1) S_D that is rigidly connected to the generating disk; (2) an auxiliary fixed coordinate system S_k wherein the motion of disk is represented; (3) coordinate system $S_1^{(2)}$ where the generated double-crowned pinion tooth surface is represented. Then, we obtain

$$\mathbf{r}_1^{(2)}(u_r, \theta_D, l_D) = \mathbf{M}_{1k}^{(2)} \mathbf{M}_{kD}(l_D) \mathbf{r}_D(u_r, \theta_D) \tag{40}$$

$$f_{1D}(\theta_D, l_D) = \tan\theta_D - l_D \left[2a_{pl} - \frac{1}{E_0 - a_{pl} l_D^2} \right] = 0 \tag{41}$$

where

$$\mathbf{M}_{kd} = \begin{bmatrix} 1 & 0 & 0 & 0 \\ 0 & 1 & 0 & -a_{pl} l_D^2 \\ 0 & 0 & 1 & l_D \\ 0 & 0 & 0 & 1 \end{bmatrix} \tag{42}$$

and

$$\mathbf{M}_{1k}^{(2)} = \begin{bmatrix} 1 & 0 & 0 & 0 \\ 0 & 1 & 0 & E_0 \\ 0 & 0 & 1 & 0 \\ 0 & 0 & 0 & 1 \end{bmatrix} \tag{43}$$

Equation (40) represents the family of disk surfaces Σ_D. Equation (41) is the equation of meshing of generating disk and double crowned pinion tooth surface $\Sigma_1^{(2)}$.

The normal to $\Sigma_1^{(2)}$ is represented in coordinate system $S_1^{(2)}$ as

$$\mathbf{n}_1^{(2)}(u_r, \theta_D, l_D) = \mathbf{L}_{1k}^{(2)} \mathbf{L}_{kD}(l_D) \mathbf{n}_D(u_r, \theta_D) \tag{44}$$

6. COMPUTERIZED SIMULATION OF MESHING AND CONTACT

The purpose of simulation of meshing and contact is investigation of influence of errors of alignment on transmission errors and shift of bearing contact. Simulation of meshing is based on an algorithm that provides continuous tangency of contacting surfaces (ref. 7). The tangency of surfaces is provided by observation of equality of position vectors and collinearity of surface normals at the instantaneous point of tangency (ref. 7). The bearing contact is simulated by the set of instantaneous contact ellipses obtained by observation of following conditions: (1) the tooth surfaces are in point contact but the contact is spread on an elliptical area due to elastic deformation of contact surfaces. The dimensions and orientation of instant contact ellipse is determined applying the relations between the surface principal curvatures and directions at the instantaneous contact point (ref. 7).

Applied Coordinate Systems

Coordinate system S_f is the fixed one and is rigidly connected to the frame of the face-gear drive (fig. 16(a)). Coordinate systems S_1 (fig. 16(a)) and S_2 (fig. 17(b)) are rigidly connected to the pinion and the face-gear, respectively. Auxiliary coordinate system S_q, S_d and S_e are applied for simulation of errors of alignment of face gear drive. All alignment errors are referred to the gear. The location of S_q with respect to S_f is shown in figure 16(b). Parameters ΔE, B, and B cot γ determine the location of origin O_q with respect to O_f (fig. 16(b)). The location and orientation of coordinate systems S_d and S_e with respect to S_q are shown in figure 17(a). The misaligned face-gear performs rotation about the z_e axis (fig. 17(b)).

Algorithm for Simulation of Meshing

Tooth surface of face-gear and its normal have been represented in S_2 by equations of three related parameters

$$\mathbf{r}_2 = \mathbf{r}_2(u_d, \theta_d, \phi_s), \qquad f_{2s}(u_d, \theta_d, \phi_s) = 0 \tag{45}$$

$$\mathbf{n}_2 = \mathbf{n}_2(u_d, \theta_d, \phi_s) \tag{46}$$

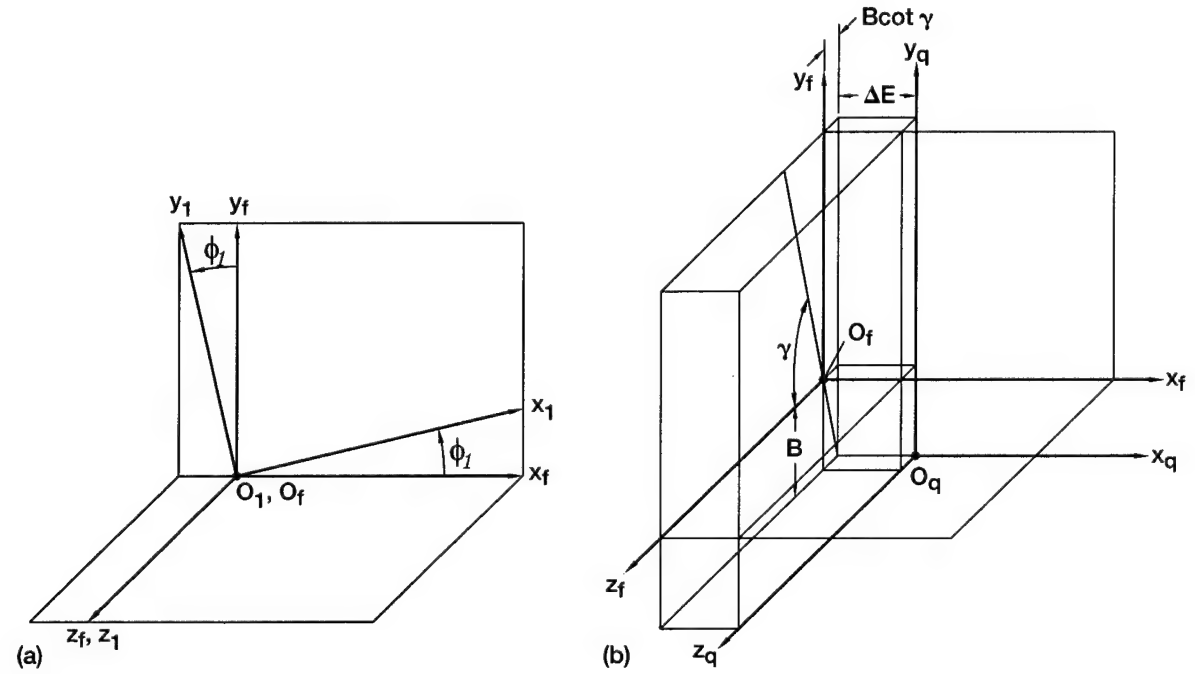

Figure 16.—Coordinate systems applied for simuation of meshing, I.

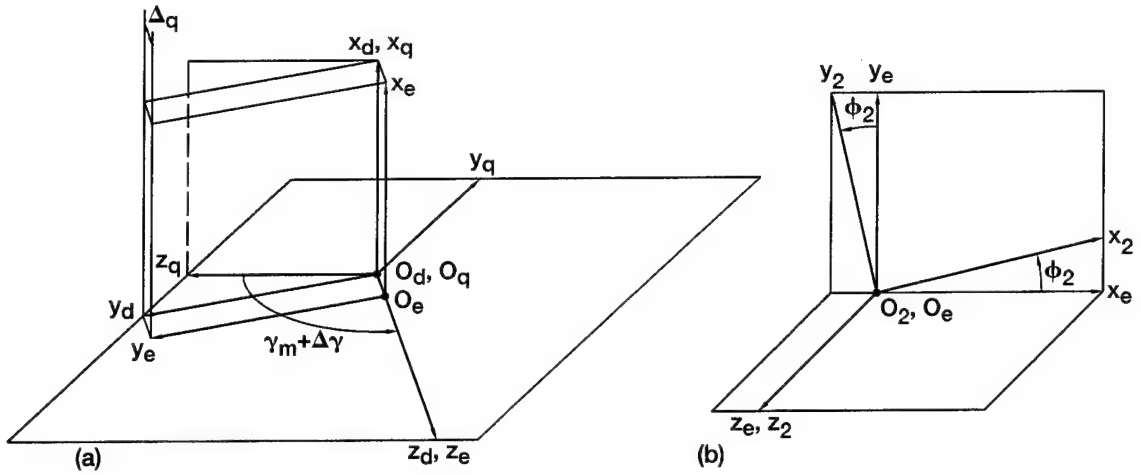

Figure 17.—Coordinate systems applied for simulation of meshing, II.

Tooth surface of double-crowned pinion and surface normal have been represented in S_1 by equations of three related parameters as well

$$\mathbf{r}_1 = \mathbf{r}_1(u_r, \theta_D, l_D), \qquad f_{1D}(u_r, \theta_D, l_D) = 0 \tag{47}$$

$$\mathbf{n}_1 = \mathbf{n}_1(u_r, \theta_D, l_D) \tag{48}$$

The superscript "(2)" in equations (47) and (48) has been dropped. The tangency of surfaces Σ_1 and Σ_2 is considered in S_f as the observation of following equations

$$\mathbf{r}_f^{(1)}(u_r, \theta_D, l_D, \phi_1) - \mathbf{r}_f^{(2)}(u_d, \theta_d, \phi_s, \phi_2) = 0 \tag{49}$$

$$\mathbf{n}_f^{(1)}(u_r, \theta_D, l_D, \phi_1) - \mathbf{n}_f^{(2)}(u_d, \theta_d, \phi_s, \phi_2) = 0 \tag{50}$$

$$f_{2s}(u_d, \theta_d, \phi_s) = 0 \tag{51}$$

$$f_{1d}(u_r, \theta_D, l_D) = 0 \tag{52}$$

Here, $\mathbf{r}_f^{(i)}$ (i = 1,2) are the surfaces of the pinion (i = 1) and the face-gear (i = 2) in fixed coordinate system S_f, and $\mathbf{n}_f^{(i)}$ (i = 1,2) are the surface unit normals of the pinion and face-gear in the same coordinate system S_f. Equations (49) to (52) yield a system of seven nonlinear equations in eight unknowns. We remind that vector equation $\mathbf{n}_f^{(1)} - \mathbf{n}_f^{(2)} = 0$ yields only two independent scalar equations, since $\left|\mathbf{n}_f^{(1)}\right| = \left|\mathbf{n}_f^{(2)}\right| = 1$. One of the unknowns, say ϕ_1, is chosen as the input parameter, and the solution of equations (49) to (52) is sought-for by functions

$$\{u_r(\phi_1), \theta_D(\phi_1), l_D(\phi_1), u_d(\phi_1), \theta_d(\phi_1), \phi_s(\phi_1), \phi_2(\phi_1)\} \in C^1 \tag{53}$$

The process of computation is an iterative process performed by application of a non-linear equation solver (ref. 4). It is assumed that there is known the first guess for solution as a set of eight parameters

$$P^{(0)}(u_r^{(0)}, \theta_D^{(0)}, l_D^{(0)}, u_d^{(0)}, \theta_d^{(0)}, \phi_s^{(0)}, \phi_2^{(0)}) \tag{54}$$

that satisfies equations (49) to (52) and the Jacobian of the system of seven equations differs at $P^{(0)}$ from zero (ref. 7), i.e.,

$$\frac{D(f_1, f_2, f_3, f_4, f_5, f_6, f_7)}{D(u_r, \theta_D, l_D, u_d, \theta_d, \phi_s, \phi_2)} \neq 0 \tag{55}$$

RESULTS OF INVESTIGATION

Simulation of meshing and contact has been performed for the following cases of design:

Case 1.—A symmetric face gear drive is considered. The face-gear is generated by an involute shaper, the pinion is a spur involute one, but the difference of number of teeth $N_S - N_1 = 3$ has been provided. Longitudinal crowning has not been accomplished.

The results of accomplished research show (fig. 18): (1) the gear drive is sensitive to change of shaft angle γ; (2) shift of bearing contact caused by $\Delta\gamma$ can be compensated by displacement Δq of the face gear in axial direction. No transmimssion errors occur in discussed case.

Case 2.—In addition to conditions of case 1, longitudinal crowning of involute pinion has been provided with parabola coefficient of plunging $a_{pl} = 0.005$ 1/in. Drawings of figure 19 show that the shift of bearing contact caused by errors of alignment $\Delta\gamma$, ΔE, and Δq can be reduced due to longitudinal crowning. However, misalignment, for instante, $\Delta\gamma$, causes a discontinuous function of transmission errors (fig. 20) that might be a source of vibrations.

Case 3.—As in cases 1 and 2, a symmetric face gear drive is considered. The face-gear is generated by an involute shaper, the pinion is profile crowned by application of an imaginary parabolic rack-cutter and is longitudinally crowned by plunging of generating disk (see section 5); the pinion and shaper have the same number of teeth ($N_s = N_1$). The bearing contact is stabilized (fig. 21), and the function of transmission errors is indeed a parabolic one and of a small magnitude (fig. 22).

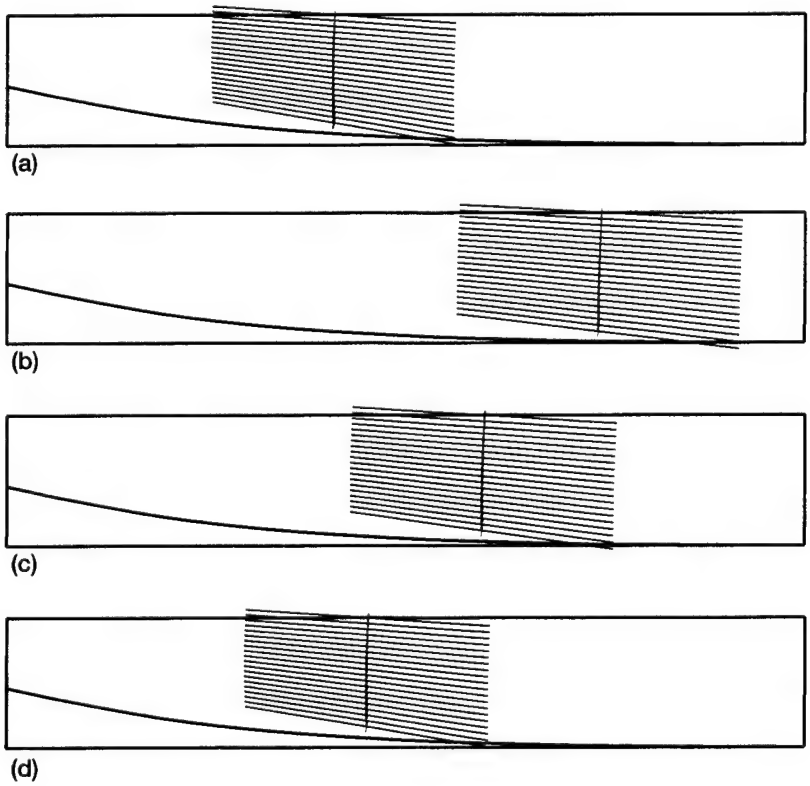

Figure 18.—Design case 1: path of contact and bearing contact for following examples. (a) No errors of errors of alignment. (b) $\Delta\gamma = 0.04$ deg. (c) $\Delta\gamma = 0.04$ deg and $\Delta q = -0.02$ mm. (d) $\Delta\gamma = 0.04$ deg and $\Delta q = -0.04$ mm.

Case 4.–An asymmetric face gear drive is considered. The face-gear is generated by an involute shaper, the pinion is profile and longitudinally crowned and the pinion and shaper have the same number of teeth ($N_s = N_1$). Larger pressure angle has been provided for the driving side of the tooth (table I). The bearing contact is stabilized for both sides, the driving and the coast ones (fig. 23).

The parameters of gear drives for all cases of design discussed above are represented in table I. The represented results of simulation of meshing and contact for the cases of design discussed above are complemented with stress analysis (section 7).

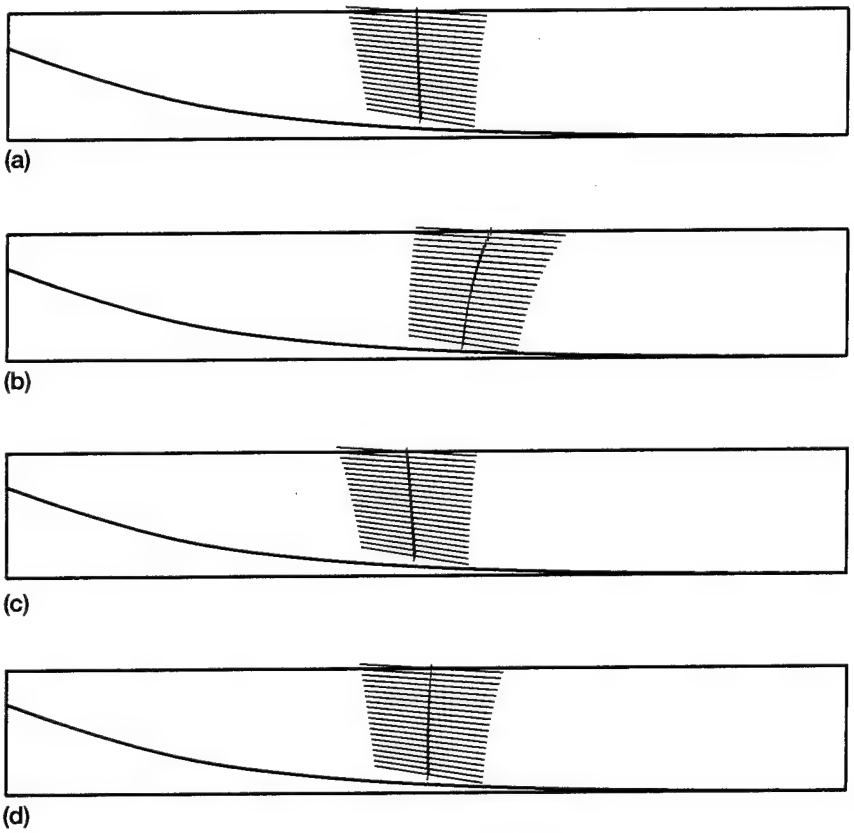

Figure 19.—Design case 2: path of contact and bearing contact for following cases. (a) No errors of errors of alignment. (b) $\Delta\gamma$ = 0.04 deg. (c) $\Delta\gamma$ = 0.01 mm. (d) $\Delta\gamma$ = 0.1 mm.

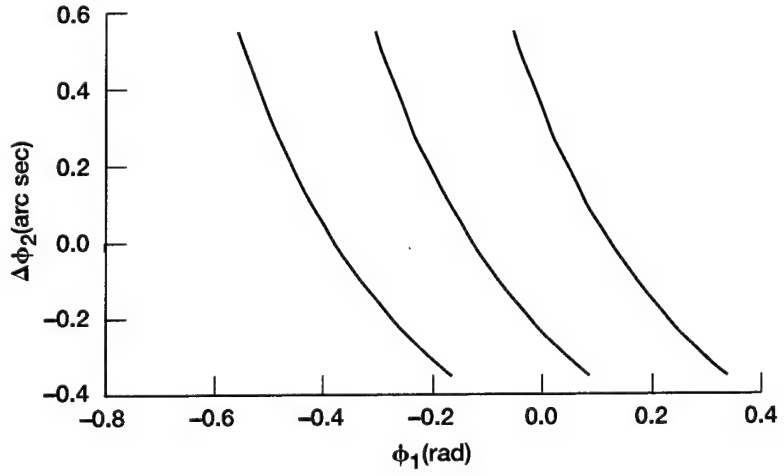

Figure 20.—Design case 2: transmission errors caused by $\Delta\gamma$ = 0.04 deg.

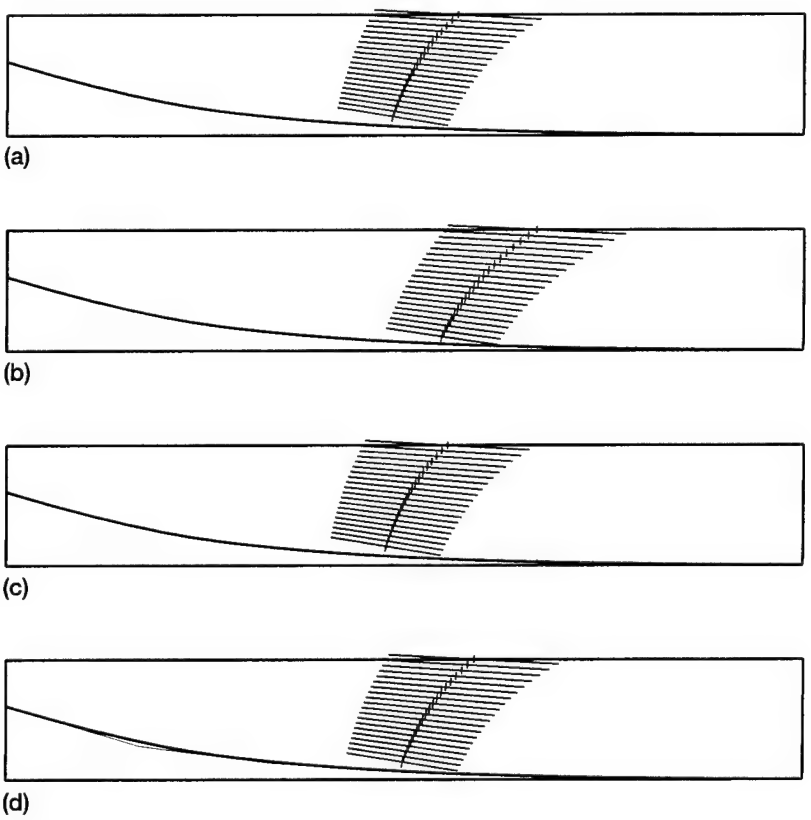

Figure 21.—Design case 3: path of contact and bearing contact for following examples. (a) No errors of errors of alignment. (b) $\Delta\gamma$ = 0.04 deg. (c) ΔE = 0.01 mm. (d) Δq = 0.1 mm.

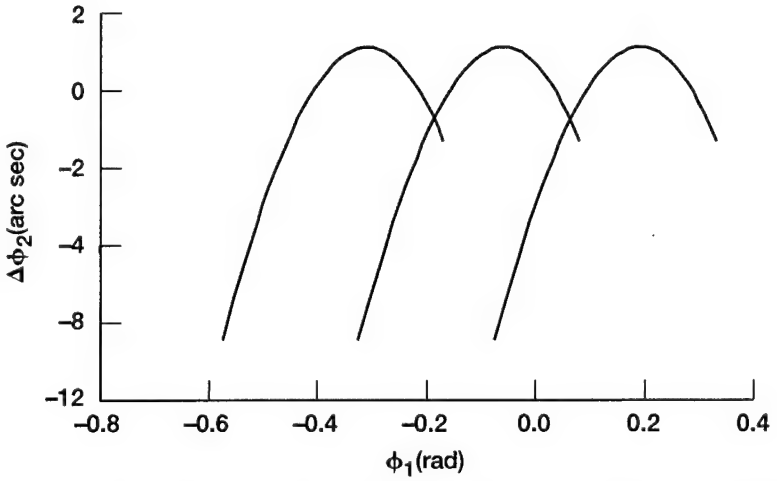

Figure 22.—Design case 3: transmission errors caused by $\Delta\gamma$ = 0.04 deg.

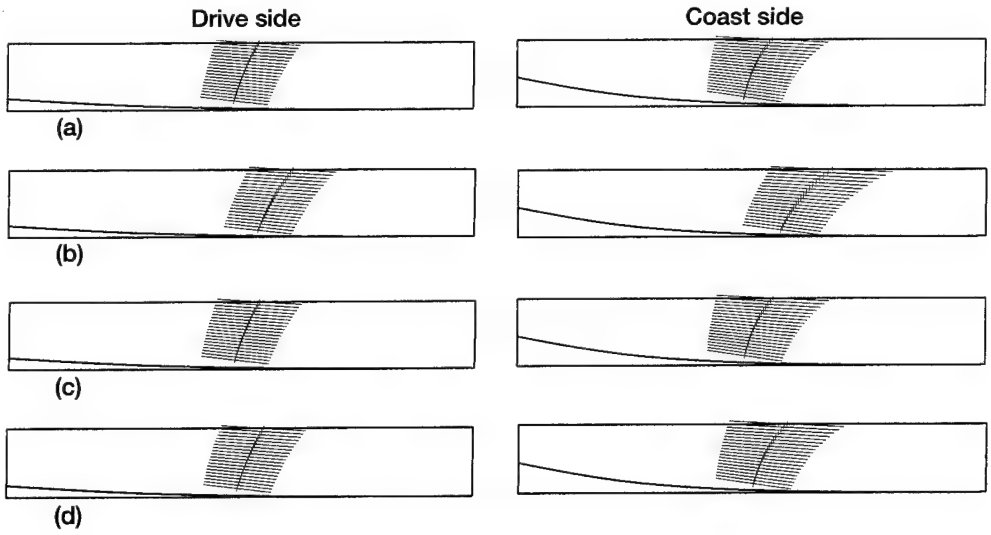

Figure 23.—Design case 4: path of contact and bearing contact for following examples. (a) No errors of errors of alignment. (b) $\Delta\gamma$ = 0.04 deg. (c) ΔE = 0.01 mm. (d) Δq = 0.1 mm.

TABLE I.—DESIGN PARAMETERS APPLIED IN CASES 1 TO 4 OF DESIGN FOR SIMULATION OF MESHING

Design parameter	Case 1	Case 2	Case 3	Case 4
Pinion tooth number, N_1	25			
Shaper tooth number, N_s	28	28	25	25
Gear tooth number, N_2	160			
Driving side pressure angle, α_d(deg.)	25.0	25.0	25.0	30.0
Coast side pressure angle, α_c(deg.)	25.0	25.0	25.0	20.0
Diametral pitch, P (in.)	5			
Shaft angle, γ (deg.)	80.0			
Coefficient of tooth thickness, λ_t (sect. 2)	1.0			
Shaper orientation angle, ξ_s (deg.) (fig. 8)	3.2143	3.2143	3.6000	3.9754
Pinion orientation angle, ξ_r(deg.)	3.6000	3.6000	3.6000	3.9754
Limiting parameter L_1(in.) (fig. 12)	19.2	19.2	19.2	20.0
Limiting parameter L_2 (in.) (fig. 12)	23.0	23.0	23.0	23.5
Rack-cutter parabola coefficient, a_r (fig. 13)	0.0	0.0	0.01	0.01
Rack-cutter parabola coefficient, a_q (fig. 13)	0.0	0.0	0.01	0.01
Parabola coefficient for plunging, a_{pl} (fig. 14)	0.0	0.005	0.005	0.005

7. STRESS ANALYSIS

Preliminary Considerations

The goals of the stress analysis represented in this section are: determination of contact and bending stresses for various cases of design of symmetric and asymmetric face-gear drives, and comparison of stresses obtained for discussed cases.

The stress analysis is based on finite element method (ref. 1). A PC version of this program running on windows NT 4.0 operating system is used to obtain the numerical solution for the contact problem by nonlinear static analysis.

The following assumptions have been accepted: (1) one pair of teeth are in mesh, (2) the friction forces are neglected, and (3) both pinion and face-gear are made of isotropic and homogeneous material. To compare the obtained results, the same finite element mesh have been designed for each considered type of geometry with the same number of nodes and elements. The same torque of 13276.8 lbf·in. has been applied to the pinion.

Eight models of contacting teeth based on the real geometry of the pinion and the face-gear tooth surfaces have been developed. This allows us to discover the contact area and compute the contact stresses. Application of TCA (Tooth Contact Analysis) for discovery of contact area and assumption about the distribution of the contact force are not required. Position of contact corresponding to $\phi_1 = 0$ has been considered for all cases.

Since the PC version of finite element analysis does not have an interactive preprocessor, a CAD package (ref. 3) is used for the development of geometric models and their meshing. These data are obtained for real geometry by application of developed computer program.

The following cases of design have been considered for finite element analysis:

- Case 1: Symmetric face gear drive, involute pinion, involute shaper, $N_s - N_1 = 3$, neither longitudinal nor profile crowning are provided.
- Case 2: Asymmetric face gear drive, involute pinion, involute shaper, $N_s - N_1 = 3$, neither longitudinal nor profile crowning are provided.
- Case 3: Symmetric face gear drive, noninvolute pinion (generated by rack-cutter of parabolic profile), involute shaper, $N_s - N_1 = 0$, longitudinal and profile crowning are provided ($a_r = 0.01$, $a_q = 0.01$, and $a_{pl} = 0.005$).
- Case 4: Asymmetric face gear drive, noninvolute pinion (generated by rack-cutter of parabolic profile), involute shaper, $N_s - N_1 = 0$, longitudinal and profile crowning are provided ($a_r = 0.01$, $a_q = 0.01$, and $a_{pl} = 0.005$).
- Case 5: Symmetric face gear drive, involute pinion, involute shaper, $N_s - N_1 = 3$, only longitudinal plunging is ($a_r = 0.0$, $a_q = 0.0$, and $a_{pl} = 0.005$).
- Case 6: Asymmetric face gear drive, involute pinion, involute shaper, $N_s - N_1 = 3$, longitudinal plunging is provided ($a_r = 0.0$, $a_q = 0.0$, and $a_{pl} = 0.005$).
- Case 7: Symmetric face gear drive, involute pinion, involute shaper, $N_s - N_1 = 1$, longitudinal plunging is ($a_r = 0.0$, $a_q = 0.0$, and $a_{pl} = 0.005$).
- Case 8: Asymmetric face gear drive, involute pinion, involute shaper, $N_s - N_1 = 1$, longitudinal plunging is provided ($a_r = 0.0$, $a_q = 0.0$, and $a_{pl} = 0.005$).

In all cases, a face gear drive with a pinion of 25 teeth and a face-gear with 160 teeth have been considered. The input design data are: diametral pitch $P = 4$ in., the shaft angle $\gamma = 80°$, and the coefficient of tooth thickness $\lambda_t = 1.0$. Wherein a symmetric face gear drive is considered (cases 1, 3, 5, and 7), the pressure angles of the driving and coast side are considered equal to 25.0° and the limiting parameters L_1 and L_2 (fig. 12) are considered equal to 19.5 and 23.0 in. respectively. In cases when an asymmetric face gear drive is considered (cases 2, 4, 6, and 8), the pressure angles of the driving and the coast sides have been taken of 30.0 and 20.0°, respectively. Limiting parameters L_1 and L_2 (Fig. 12) have been taken of 20.0 and 23.0 in., respectively, to avoid undercutting of the coast side.

Developed Geometric Models and Boundary Conditions

The developed finite element three-dimensional models are shown in figures 24 and 25 for the symmetric and asymmetric face-gear drives, respectively. First order brick elements have been used to build the global finite element mesh. The total number of elements is 14344 with 21386 nodes for each geometric model. The material is steel with the properties of Young's Modulus $E = 3\times10^7$ lbf/in.^{2} and the Poisson's ratio $\nu = 0.29$.

As it was mentioned above, the models have been developed by application of a geometric modeling program and then transferred for stress analysis. Two options related to the contact problem, "small sliding" and "no friction," have been selected.

One of the finite element method advantages in comparison with other finite element programs is the use of pure master-slave contact algorithm easily defined from exported data of the the geometric model. Pure master-slave contact algorithm means that nodes on the slave surface cannot penetrate the master surface. Generally, the master surface should be chosen as the surface of the stiffer body or as the surface with the coarser mesh if the two surfaces

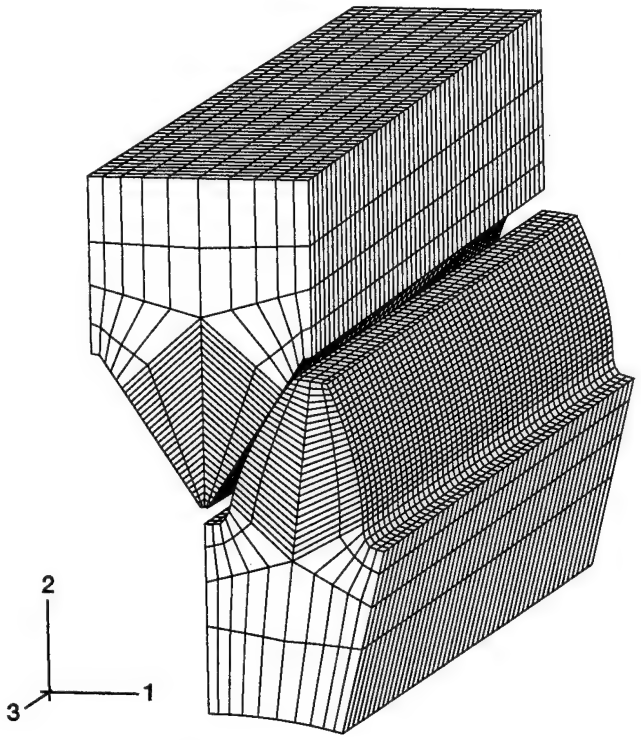

Figure 24.—3D finite element model for symmetric face-gear drive.

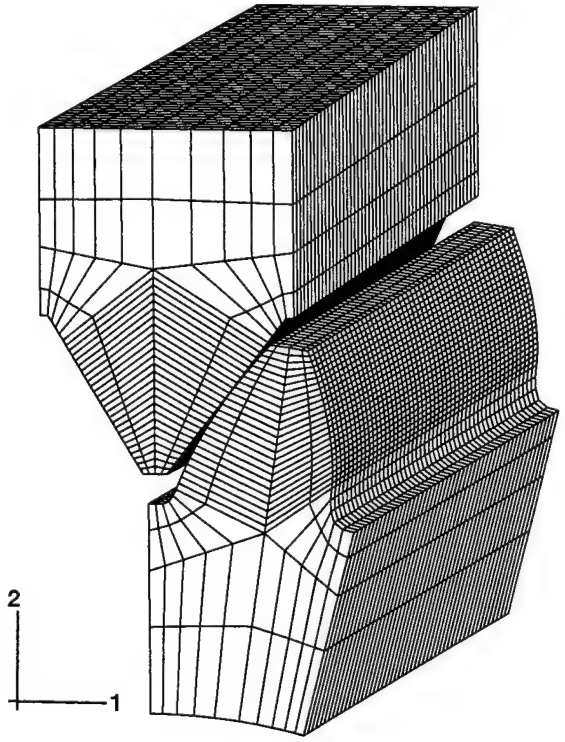

Figure 25.—3D finite element model for asymmetric face-gear drive.

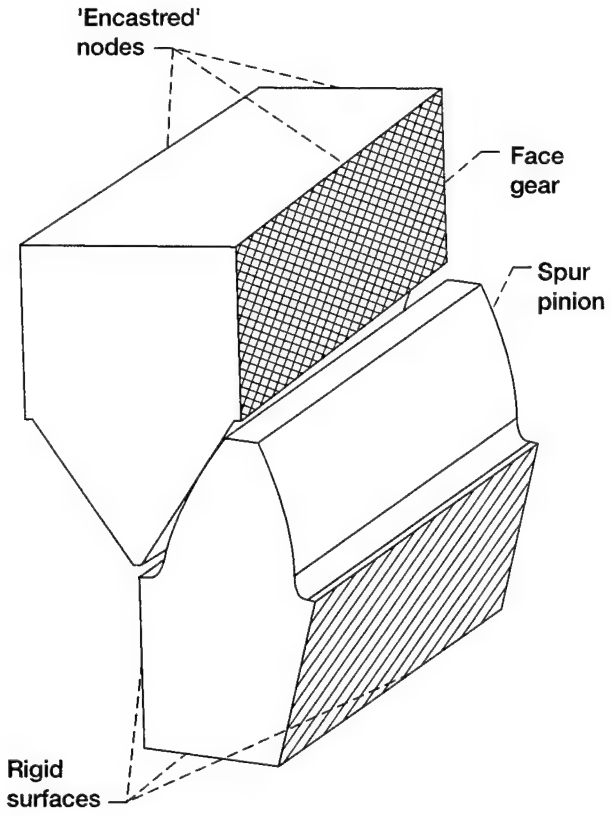

Figure 26.—Boundary conditions for the pinion and face-gear.

are on structures with comparable stiffness. The stiffness of the structure and not just the material should be considered when choosing the master and slave surface. The mesh density on both pinion and face-gear are the same. It has been supossed that the stiffness of the face-gear structure is larger in comparison with the pinion. Therefore, the face-gear and pinion surfaces have been chosen as the master surface and the slave, respectively.

A new approach to set up boundary conditions has been applied. Nodes on the two outer and inner sides of the face-gear base cube are considered "encastred" (six degrees of freedom are considered equal to zero). Nodes on the two outer sides and the base of the pinion cube build a rigid surface (fig. 26). Surfaces of this type are three-dimensional geometric structures that cannot be deformed but can perform translation or rotation as rigid bodies. They are also very cost-effective since the variables associated with a rigid surface are the translations and rotations of a single node, known as the rigid body reference node (fig. 27).

Using this approach, we can apply the torque directly to the rigid body reference node located on the pinion axis of rotation (fig. 27). The remaining five degrees of freedom of the rigid reference node are restricted to be zero.

RESULTS OF INVESTIGATION

Minimum principal stresses in the area of contact are considered as compressive stresses. Maximum principal stresses are considered as tensile stresses. The finite element analysis considers SP3 ≥ SP2 ≥ SP1 corresponding to $\sigma_1 \geq \sigma_2 \geq \sigma_3$ in classical principal-stress theory.

The numerical results are summarized in table II.

Figures 28 and 29 show the contact and bending stresses for the face gear of symmetric face-gear drive described as case 1, respectively.

The obtained results may be summarized as follows:

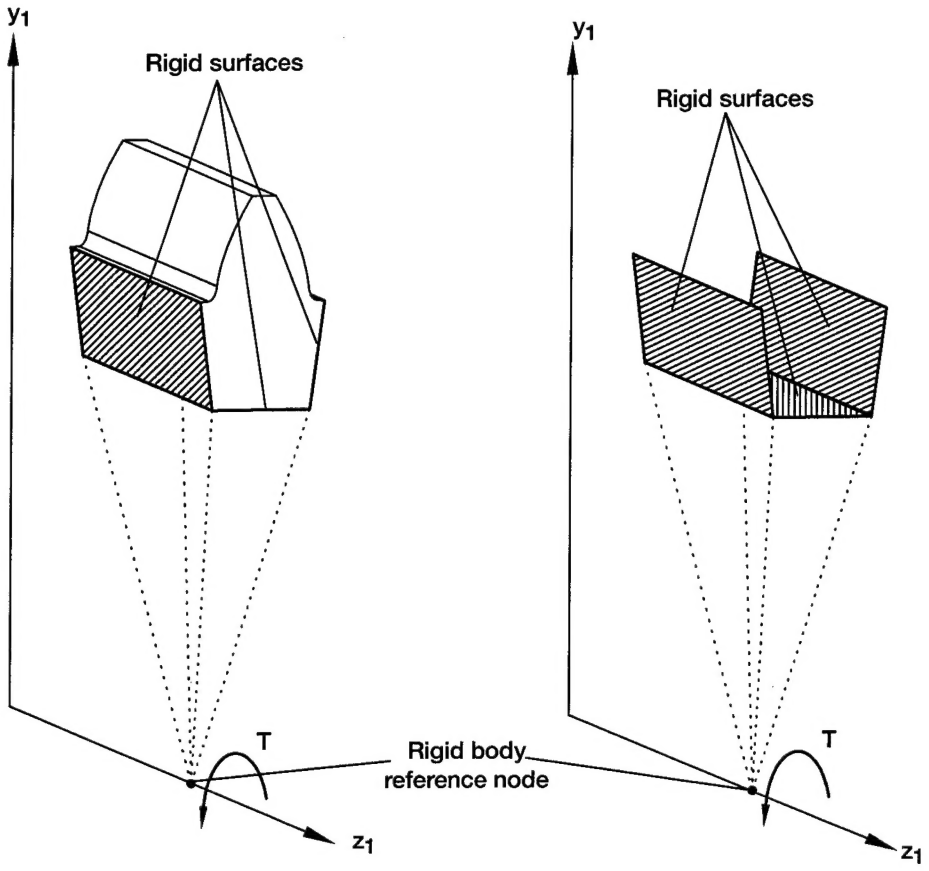

Figure 27.—Rigid surfaces for boundary conditions for the pinion.

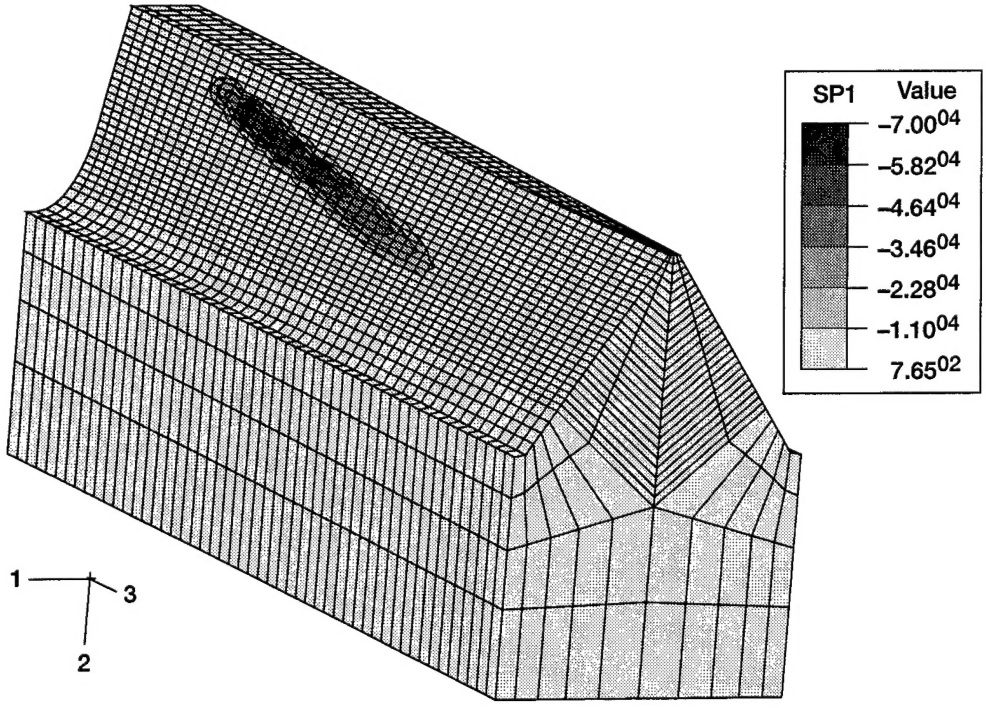

Figure 28.—Case 1 finite element analysis; contact stresses for symmetric face-gear drive.

TABLE II.—RESULTS OF THE FINITE ELEMENT ANALYSIS

	Case 1	Case 2	Case 3	Case 4
Pinion max. cont. stress SP1 (kpsi)	–71.0	–59.9	–107.0	–128.0
Pinion max. bend. stress SP3 (kpsi)	25.5	18.8	31.5	28.4
Face gear max. cont. stress SP1 (kpsi)	–70.0	–72.0	–102.0	–110.0
Face gear max. bend. stress SP3 (kpsi)	19.8	17.2	22.4	21.1
	Case 5	Case 6	Case 7	Case 8
Pinion max. cont. stress SP1 (kpsi)	–129.0	–116.0	–133.0	–114.0
Pinion max. bend. stress SP3 (kpsi)	32.1	28.7	30.6	28.1
Face gear max. cont. stress SP1 (kpsi)	–121.0	–110.0	–93.9	–104.0
Face gear max. bend. stress SP3 (kpsi)	25.8	23.7	24.1	22.0

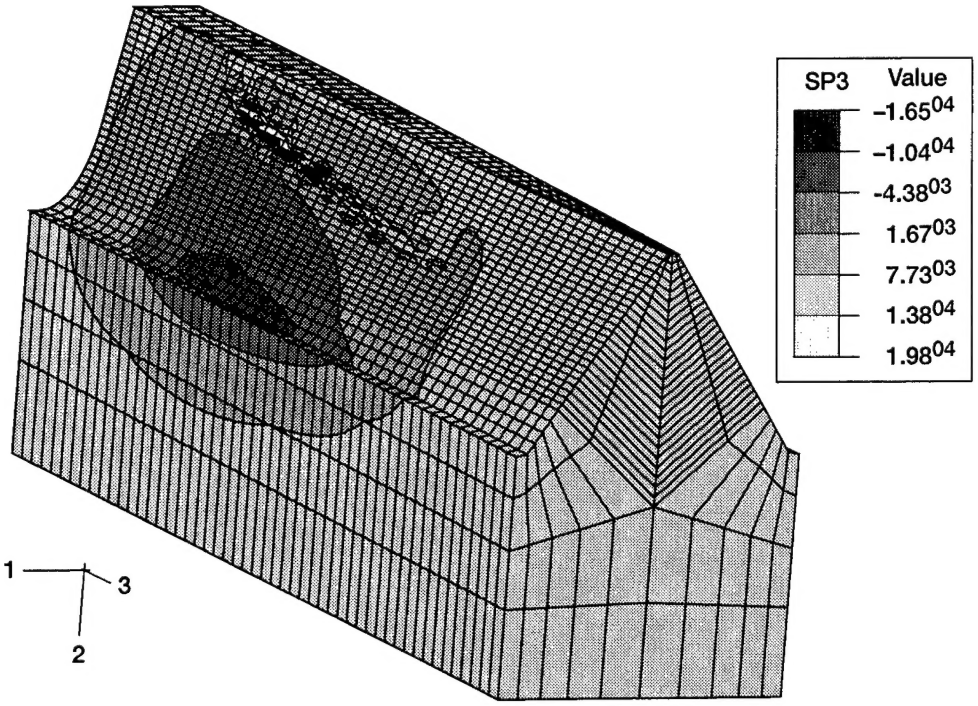

Figure 29.—Case 1 finite element analysis; bending stresses for symmetric face-gear drive.

(1) The lowest stresses may be obtained for an asymmetric gear drive with an involute pinion and involute shaper applied for generation of face gear. However, the gear drive is sensitive to error $\Delta\gamma$ of shaft angle. The shifted bearing contact may be restored by respective regulation of axial location of the face-gear, by regulation of Δq (see fig. 17). The great advantage of this design is that the transmission errors of the gear drive are zero.

(2) Application of double crowned pinion is favorable for stabilization of bearing contact, but stresses are increased. Therefore, this type of modified geometry is preferable for low-loaded gear drives.

8. CONCLUSIONS

Based on the performed research, the following conclusions can be drawn:

(1) The geometry of a new type of asymmetric face gear drive has been developed.

(2) Simulation of meshing and contact of misaligned symmetric and asymmetric face gear drives has been developed.

(3) Generation of the face gear with a shaper with increased number of teeth and application of a larger pressure angle for the driving side is proposed to reduce both contact and bending stresses in the pinion denture. Axial displacement of the face-gear, Δq, may be used to restore the bearing contact to the desired position on the face-gear tooth surface. There are no transmission errors in case of application of involute shaper and involute pinion.

(4) Double-crowned pinion for the drive can be used to provide a localized bearing contact and a parabolic function of transmission errors wherein errors of alignment exist. However, bending and contact stresses of the pinion and face-gear will be increased in comparison with versions of design discussed above.

(5) Stress analysis by application of finite element analysis has been accomplished for symmetric and asymmetric face gear drives. The reduction of both contact and bending stresses of more than 10 percent has been confirmed for asymmetric face gear drives.

(6) Computer programs for the design and analysis of the conventional and the new type of geometry of an asymmetric face gear drive, have been developed.

REFERENCES

1. ABAQUS/Standard 5.8 User's Manual, Hibbitt, Karlsson & Sorensen, Inc.
2. Favard, J.: Course of Local Differential Geometry, Gauthier-Villars, Paris (in French, translated into Russian), 1957.
3. I-Deas Master Series Manual, SDRC Part No P–50002, Structural Dymanics Research Corporation.
4. IMSL Math/Library: User's Manual, MALB-USM-UNBND-EN8901–1.1,2500, Citynest Bl. Houston, Texas.
5. Korn, G.A., Korn, T.M.: Mathematical Handbook for Scientists and Engineers, 2nd ed. McGraw-Hill, NY, 1968.
6. Litvin, F.L., Lian, Q., Kapelevich, A.L.: Asymmetric Modified Spur Gear Drives: Reduction of Noise, Localization of Contact, Simulation of Meshing and Stress Analysis, Computer Methods in Applied Mechanics and Engineering, 188, pp. 363–390, 2000.
7. Litvin, F.L.: Gear Geometry and Applied Theory, Prentice Hall, 1994.
8. Litvin, F.L., Egelja, A., Tan, J., and Heath, G.: Computerized Design, Generation and Simulation of Meshing of Orthogonal Offset Face-Gear Drive with a Spur Involute Pinion with Localized Bearing Contact, Mechanism and Machine Theory, Vol. 33, 1998.
9. Litvin, F.L., Wang, J.-C., Chen, Y.-J.D., Bossler, R.D., Heath, G., and Lewicki, D.J.: Face-Gear Drives: Design, Analysis and Testing for Helicopter Transmission Applications, AGMA Paper 92FTM2, 1992.
10. Litvin, F.L., Zhang, Y., Wang, J.-C., Bossler, R.B., and Chen, Y.-J.D.: Design and Geometry of Face-Gear Drives, ASME J. Mech. Design, 114, 1992.
11. Zalgaller, V.A.: Theory of Envelopes, Publishing House Nauka, Moscow, (in Russian), 1975.
12. Zalgaller, V.A., and Litvin, F.L.: Sufficient Condition of Existence of Envelope to Contact Lines and Edge of Regression on the Surface of the Envelope to the Parametric Family of Surfaces, Proceedings of Universities: Mathematics, No. 3(178):20–23, (in Russian), 1977.

REPORT DOCUMENTATION PAGE

Form Approved
OMB No. 0704-0188

1. AGENCY USE ONLY (*Leave blank*)	2. REPORT DATE	3. REPORT TYPE AND DATES COVERED
	January 2001	Technical Memorandum

4. TITLE AND SUBTITLE

Design, Generation and Tooth Contact Analysis (TCA) of Asymmetric Face Gear Drive With Modified Geometry

5. FUNDING NUMBERS

WU–581–30–13–00
1L162211A47A

6. AUTHOR(S)

Faydor L. Litvin, Alfonso Fuentes, J. Matthew Hawkins, and Robert F. Handschuh

7. PERFORMING ORGANIZATION NAME(S) AND ADDRESS(ES)

National Aeronautics and Space Administration
John H. Glenn Research Center
Cleveland, Ohio 44135–3191
and
U.S. Army Research Laboratory
Cleveland, Ohio 44135–3191

8. PERFORMING ORGANIZATION REPORT NUMBER

E–12573

9. SPONSORING/MONITORING AGENCY NAME(S) AND ADDRESS(ES)

National Aeronautics and Space Administration
Washington, DC 20546–0001
and
U.S. Army Research Laboratory
Adelphi, Maryland 20783–1145

10. SPONSORING/MONITORING AGENCY REPORT NUMBER

NASA TM—2001-210614
ARL–TR–2373

11. SUPPLEMENTARY NOTES

Faydor L. Litvin and Alfonso Fuentes, Gear Research Center, Department of Mechanical Engineering, University of Illinois at Chicago, Chicago, Illinois; J. Matthew Hawkins, Rolls-Royce, Allison Engine Company, Indianapolis, Indiana; Robert F. Handschuh, U.S. Army Research Laboratory, NASA Glenn Research Center. Responsible person, Robert Handschuh, organization code 5950, 216–433–3969.

12a. DISTRIBUTION/AVAILABILITY STATEMENT

Unclassified - Unlimited
Subject Category: 37 Distribution: Nonstandard

Available electronically at http://gltrs.grc.nasa.gov/GLTRS

This publication is available from the NASA Center for AeroSpace Information, 301–621–0390.

12b. DISTRIBUTION CODE

13. ABSTRACT ***(Maximum 200 words)***

A new type of face gear drive for application in transmissions, particularly in helicopters, has been developed. The new geometry differs from the existing geometry by application of asymmetric profiles and double-crowned pinion of the face gear mesh. The paper describes the computerized design, simulation of meshing and contact, and stress analysis by finite element method. Special purpose computer codes have been developed to conduct the analysis. The analysis of this new type of face gear is illustrated with a numerical example.

14. SUBJECT TERMS

Gears; Gear drives; Transmissions

15. NUMBER OF PAGES
36

16. PRICE CODE
A03

17. SECURITY CLASSIFICATION OF REPORT	18. SECURITY CLASSIFICATION OF THIS PAGE	19. SECURITY CLASSIFICATION OF ABSTRACT	20. LIMITATION OF ABSTRACT
Unclassified	Unclassified	Unclassified	